Mutational analysis reveals how the essential interactions of a ClpP proteolytic system regulate the apicoplast proteome in malaria parasites

Florentin A.[1,2], Stephens D.R.[2,3], Brooks C.F.[1,2], Baptista R.P.[2,4], Muralidharan V[1,2,#]

[1]Department of Cellular Biology
[2]Center for Tropical and Emerging Global Diseases
[3]Department of Pharmaceutical and Biomedical Sciences, College of Pharmacy
[4]Institute of Bioinformatics
University of Georgia, Athens, GA 30602, USA

[#]Address correspondence to: vasant@uga.edu

Abstract

The human malaria parasite, *Plasmodium falciparum*, contains a plastid called the apicoplast that functions to produce essential metabolites. Most of apicoplast proteins are encoded by the nuclear genome and it is unclear how the apicoplast controls its own proteome. Here, we investigated the apicoplast caseinolytic-protease (Clp) system and how it regulates organelle proteostasis. Our data show that interfering with expression, activity or interactions of the Clp protease (PfClpP), chaperone (PfClpC), non-catalytic subunit (PfClpR), or potential substrate adaptor molecule (PfClpS) results in parasite death because of apicoplast loss. Using conditional null-mutants, we demonstrated that PfClpP is essential due to its role in apicoplast biogenesis. Conditional knockdown mutants of PfClpP revealed the robustness of its proteolytic activity and its interaction with the chaperone PfClpC. A CRISPR/Cas9 based system was developed and used for the expression of a PfClpC variant with a mutation in the putative protease binding site, which led to the discovery of its essential interaction with PfClpP. A combination of several tagged Clp proteins was used for affinity purification and determined complex composition as well as identify putative substrates. Expression of a catalytically-dead variant of PfClpP in the background of PfClpP conditional mutants showed that PfClpP oligomerizes as a zymogen and that the pro-domain is removed via trans-autocatalysis. Conditional knockdown mutants of PfClpS demonstrated its essential function in plastid biogenesis and its interaction with PfClpR as well as putative substrates. This comprehensive study reveals the molecular interactions driving the function of the apicoplast PfClpP/R/C/S system and demonstrates its central role in the biogenesis of the plastid in malaria parasites.

35 # Introduction

36 The deadly malaria parasite, *Plasmodium falciparum*, has developed resistance to all currently
37 available therapies, making the discovery of new drug targets a top priority. Like most other
38 apicomplexans, this eukaryotic parasite contains a plastid called the apicoplast[1]. This unique
39 organelle evolved via a two-step endosymbiosis[2]; in the primary endosymbiotic event, a
40 cyanobacterium was incorporated into a eukaryotic cell to form the modern chloroplast.
41 During the secondary endosymbiotic event, a photosynthetic red alga was further taken up by
42 a protist and led to the formation of a secondary plastid[3]. Although not photosynthetic, the
43 apicoplast harbors essential prokaryotic metabolic pathways that are essential to the parasite
44 throughout its complex life cycle[4]. In a sharp contrast with its human host, the *Plasmodium*
45 apicoplast shares molecular features with prokaryotes, plants and parasites, and therefore has
46 the potential to encompass multiple parasite-specific drug targets[5,6]. Indeed, drugs that target
47 apicoplast biology are in clinical use[7,8]. Most of those drugs (e.g. Doxycycline, Clindamycin)
48 target the prokaryotic protein synthesis machinery in the apicoplast[9,10]. However, less than
49 10% of the apicoplast proteome is encoded by its own genome. The vast majority of the
50 hundreds of apicoplast proteins are encoded in the nuclear genome and are transported to the
51 organelle via the secretory pathway[11-13]. Available data suggest that the apicoplast does not
52 control the translation of these nuclear encoded proteins, and, in fact, parasites without an
53 apicoplast continue to express and accumulate these proteins in vesicle-like structures in the
54 cytoplasm[14,15].

55 Due to the inability of the apicoplast to control its own protein synthesis, it is likely that it
56 maintains a stable proteome through protein degradation. This requires an organelle specific
57 proteolytic machinery that has not yet been identified. We hypothesize that this function is
58 executed by Clp (Caseinolytic protease) proteins. This family of proteins consists of ClpP
59 proteases that form multi-subunit proteolytic complexes, though the complex composition
60 varies widely between different species and organelles[16,17]. The ClpP proteases associate with
61 Clp ATPase chaperones that unfold and feed substrates into the ClpP barrel-like cavity for
62 degradation[18,19]. In bacteria, they play pivotal roles in cell division, transport, stress response
63 and virulence[20]. In plants chloroplasts, Clp proteins regulate the levels and activities of

64 numerous metabolic enzymes and thus control chloroplast metabolism and differentiation[21].
65 Some of these metabolic pathways, such as isoprenoids biosynthesis, are conserved and
66 essential in the apicoplast.
67 Several putative Clp genes have been localized to the apicoplast of *P. falciparum*, but little is
68 known about their roles in apicoplast biology or their essentiality for parasite asexual life
69 cycle[22]. The putative *Plasmodium* Clp genes differ significantly from their bacterial orthologs
70 and it is unclear whether they interact or even form a complex. They also include a putative
71 noncatalytic subunit termed PfClpR that is absent in most bacteria[23]. We have previously
72 shown that the *Plasmodium* ClpC chaperone (PfClpC) is essential for parasite viability and
73 apicoplast biogenesis[15]. Here, we report the development and application of advanced
74 molecular genetic tools in a clinically important non-model organism to gain detailed
75 mechanistic insights into plastid Clp function and how this drives parasite biology. Collectively,
76 these data demonstrate that the Clp complex and interactions within this proteolytic system
77 acts as an essential nexus regulating apicoplast biogenesis.

Results and Discussion

PfClpP is essential for apicoplast biogenesis and survival of malaria parasites

In order to assess the biological role of the *Plasmodium* ClpP homolog, PfClpP, and test its potential as a drug target, we attempted to generate a null mutant, replacing the *pfclpp* gene with a drug marker using CRISPR/Cas9 gene editing (Figure 1A). Despite PCR evidence for successful integration into the *pfclpp* locus (Supplementary Figure 1), we repeatedly failed to retrieve live parasites following drug selection. This suggested that PfClpP is essential for parasite viability and we therefore decided to repeat the transfection in the presence of isopentenyl pyrophosphate (IPP). IPP is a small metabolite produced by the apicoplast which was shown to be the only essential function of the organelle during the asexual blood stages[14]. Transfection in the presence of IPP yielded live PfClpP knockout parasites (PfClpP^{KO}) on the first attempt, and integration was confirmed by PCR (Figure 1B). Using an anti-PfClpP antibody we verified that PfClpP^{KO} mutants do not express PfClpP (Figure 1C). Removal of IPP from the culturing media resulted in the rapid death of the PfClpP^{KO} parasites (Figure 1D). Immuno-fluorescence assays (IFA) revealed that apicoplast proteins such as Acyl Carrier Protein (ACP) and Chaperonin 60 (Cpn60) lost their typical apicoplast localization, and instead appear in vesicle-like structures (Figure 1E). Such structures are indicative of damage to organelle integrity. Indeed, quantitative Real Time PCR (qRT-PCR) showed that the entire apicoplast genome disappeared in PfClpP^{KO} mutants, while the mitochondria genome was unaffected (Figure 1F). Collectively, these data demonstrate that PfClpP is essential for parasite viability, and its function is required for the biogenesis of the apicoplast organelle.

PfClpP knockdown reveals robust enzymatic activity *in vivo*

Next, we wanted to investigate the molecular mechanisms of PfClpP function. To do that, we tagged the gene with a V5 tag and the *tetR*-aptamer conditional knockdown (KD) system, enabling translational repression of PfClpP expression when anhydrotetracycline (aTc) is removed from the culturing media[24]. Using CRISPR/Cas9, we incorporated the *tetR*-aptamer regulatory cassette at the 3'end of the *pfclpp* gene, creating the PfClpP^{apt} parasite line (Figure 2A). Using PCR analysis, we verified correct integration into the *pfclpp* locus (Figure 2B), and by

107 IFA we confirmed its apicoplast localization (Figure 2C). Western blot analysis revealed the
108 expected processing pattern of PfClpP; cytoplasmic fraction (I); apicoplast-localized zymogen
109 (II) and a mature protease after proteolytic removal of the pro-domain (III) (Figure 2D)[15,22].
110 Inducing knockdown by removing aTc resulted in a significant reduction (>95%) in PfClpP
111 protein levels, however this reduction had no effect on parasite growth (Figure 2D and E). This
112 indicated that residual PfClpP protein levels were sufficient to maintain biologically functional
113 enzymatic activity without any deleterious effects. The fact that PfClpP is essential for
114 apicoplast function, and its maturation is proteolytically controlled, raised the possibility that it
115 is post-translationally regulated.
116
117 **The PfClpP and PfClpR bind each other and share common interacting partners**
118 Another putative member of the plastid Clp complex and a potential regulator of PfClpP
119 activity is PfClpR, a potential non-catalytic subunit in the Clp complex[22,23]. We therefore
120 attempted to tag PfClpR with the V5 tag and the *tetR* aptamer knockdown system
121 (Supplementary Figure 2A). Tagging *pfclpr* locus has been challenging[15] and after multiple
122 attempts, we finally succeeded in tagging the locus with the *tetR* aptamer. However, PCR
123 analysis of the aptamer repeats region in PfClpR^{apt} parasites, revealed that the number of
124 aptamer repeats decreased during drug selection from 10 to 7 (Supplementary Figure 2B). This
125 significantly compromised knockdown efficiency and prevented us from evaluating its effect
126 on parasite replication (Supplementary Figure 2C). We concluded that tagging this locus
127 confers a fitness cost and that, like PfClpP, PfClpR may be essential for plastid biogenesis.
128 Nevertheless, the PfClpR gene was correctly tagged with the V5 epitope and, like PfClpP, was
129 localized to the apicoplast (Supplementary Figure 2D). It is interesting to note that the non-
130 catalytic PfClpR comprises an inactive Clp protease domain, but does not have a pro-domain,
131 and migrates similarly on SDS-PAGE as the mature PfClpP (Supplementary Figure 2E).
132 In order to identify other potential Clp interactors and regulators, we performed
133 immunoprecipitation (IP) of PfClpP^{apt} and PfClpR^{apt} parasites using the V5 tag. For large scale
134 proteomic analyses, potential Clp interactors were isolated from non-synchronized PfClpP^{apt}
135 and PfClpR^{apt} parasites using anti-V5 antibody-conjugated beads. The parental line (3D7) was

136 used as a control, and all samples were analyzed by mass spectrometry. All detected proteins
137 were filtered for predicted apicoplast localization and the abundance of each apicoplast-
138 predicted protein was calculated and averaged between biological replicates. Using individual
139 peptide abundance values, we calculated a ratio between protein abundance in IP (PfClpP or
140 PfClpR) and the parental control and set a threshold of ≥5-fold enrichment (Figure 2F and G).
141 This resulted in a list of proteins that were either detected exclusively in the Clp IP or were at
142 least 5- fold or more abundant than in the control. PfClpP IP yielded 45 proteins that are
143 predicted to localize to the apicoplast, and 29 out of these passed the threshold and were
144 considered high-confidence PfClpP interactors (Figure 2F and supplementary table 1). For
145 PfClpR, out of 29 apicoplast-predicted proteins, only 8 passed the threshold and were
146 considered probable PfClpR interactors (Figure 2G and supplementary table 1). Importantly,
147 PfClpR appeared as a high-confidence interactor for PfClpP and vice versa, suggesting a
148 physical interaction between the two components of the Clp complex. Moreover, 7 out of the 8
149 PfClpR positive hits were also found in the PfClpP interactors list, further reinforcing them as
150 high-confidence interactors (Figure 2H). One of these seven proteins is chaperonin 60 (Cpn60),
151 which functions in folding of proteins transported to plastids[25]. The interaction of Cpn60 with
152 the Clp complex suggests that these proteins may function as a protein quality control
153 mechanism in the apicoplast to degrade damaged and misfolded proteins.
154
155 **PfClpC interacts with mature PfClpP in the apicoplast**
156 The IP approach relied primarily on strong protein-protein interactions and could not detect
157 weaker or transient interactions with potential biological significance. For example, the mass
158 spectrometry results did not identify any Clp chaperone that may interact with the complex.
159 While the *Plasmodium* genome does not encode typical bacterial chaperones such as ClpA or
160 ClpX, it does express an atypical AAA+ ATPase termed PfClpC with a potential tripeptide ClpP
161 binding sequence[15,22]. In order to study factors such as PfClpC, we wanted to express potential
162 PfClpP regulators *in vivo* in PfClpP^{apt} parasites. For this purpose, we developed a novel,
163 modular tool for stable expression of tagged proteins in *P. falciparum*, that avoids the
164 inconsistent overexpression that occurs when using episomal plasmids. In this method, we use

165 CRISPR/Cas9 editing to insert the gene of interest into a specific genomic locus, where it is
166 expressed under an endogenous promoter. We chose the *pfhsp110c* locus, that encodes an
167 essential cytoplasmic protein that is consistently expressed throughout the parasite life
168 cycle[26]. To test whether the Hsp110 system can drive expression of apicoplast localized
169 proteins, we introduced a 2A skip peptide at the end of the gene, followed by a GFP reporter
170 with an apicoplast transit peptide (tp) derived from acyl carrier protein (ACP)[11] (tp^{ACP}-GFP,
171 Figure 3A). Transfection and integration into the into *the pfhsp110c* locus were efficient, and
172 using IFA we confirmed robust GFP expression in the apicoplast of all clones isolated (Figure
173 3B). Western blot analysis revealed the typical double-band, consisting of a weak upper band
174 of the cytoplasmic fraction and a more prominent lower band of the apicoplast localized GFP
175 after removal of the transit peptide (Figure 3C). We concluded that this method works well for
176 expression of apicoplast proteins, and can be used to study PfClpP-PfClpC interactions.
177 Using the Hsp110 expression system, we designed and expressed two isoforms of PfClpC in
178 $PfClpP^{apt}$ parasites (Figure 3A). The first was a copy of wild type PfClpC ($PfClpC^{wt}$) with a C-
179 terminal 3xTy tag. We transfected $PfClpC^{wt}$, and confirmed its co-expression with PfClpP-V5 by
180 western blot (Figure 3D, left lane) and their co-localization in the apicoplast by IFA (Figure 3F,
181 upper panel). Importantly, PfClpP pulldown resulted in the co-immunoprecipitation of
182 $PfClpC^{wt}$, indicating a physical interaction between the chaperone and the protease (Figure 3E,
183 left). The reciprocal PfClpC pulldown revealed that the chaperone interacts with the mature
184 protease (III) but not with the zymogen form (II) or the full length PfClpP with the transit
185 peptide (I) (Figure 3E, right). This indicates that PfClpC and PfClpP interact only upon co-
186 localization in the apicoplast and after the proteolytic maturation of the protease.
187
188 **The Clp chaperone-protease interaction is essential for plastid biogenesis and parasite**
189 **survival**
190 The second PfClpC variant that we expressed via the Hsp110 system had a single point
191 mutation in the 3rd amino acid of a Leu-Gly-Phe motif (aa 1101-1103) that may be required for
192 binding PfClpP (F1103W, Figure 3A)[19]. Aside from that mutation, this construct, termed
193 $PfClpC^{F1103W}$, was identical to the first ($PfClpC^{wt}$) and was similarly tagged with 3xTy and

194 expressed from the *pfhsp110c* locus in PfClpP^{apt} parasites, without interfering with the
195 endogenous *pfclpc* gene (Figure 3A). Unexpectedly, multiple attempts to express the
196 PfClpC^{F1103W} variant failed, suggesting that the mutated allele has a dominant negative effect
197 on parasite viability. To rule out a general cytotoxic effect of transfection or any putative lethal
198 consequences of interfering with PfHsp110c expression, we repeated transfections in the
199 presence of the essential apicoplast metabolite, IPP. Transfection of PfClpC^{F1103W} in the
200 presence of IPP has enabled us to retrieve live parasites. Western blot analysis revealed that in
201 these parasites, all processing of PfClpP was abolished and the only observed band was the
202 full-length cytoplasmic fraction (Figure 3D, right lane). Using microscopy, we observed that
203 both PfClpP^{apt} and PfClpC^{F1103W} did not appear in their typical apicoplast localization, and
204 instead form vesicle-like structures indicative of apicoplast damage (Figure 3F, lower panel).
205 Clones were isolated but their growth was entirely dependent on IPP, and removing it led to
206 parasites death (Figure 3G). Subsequently, quantitative real time PCR analysis revealed that
207 the apicoplast genome disappeared from PfClpC^{F1103W} parasites (Figure 3H). These results
208 indicate that interfering with the interaction between the PfClpC chaperone and the PfClpP
209 protease inhibits complex function. Furthermore, our data suggest that PfClpC dynamically
210 interacts with PfClpP and this essential interaction may be required for degradation of
211 substrates to ensure apicoplast biogenesis. To our knowledge, this is the first time that this
212 interaction has been shown to be required for any plastid biogenesis.
213
214 **PfClpP oligomerizes as a zymogen and matures via trans-autoprocessing**
215 The *Plasmodium* ClpP differs structurally from its bacterial orthologues primarily because it
216 contains a transit peptide and a pro-domain (Figure 2D), both of which are removed at
217 subsequent maturations steps. Like other proteins that are transported to the plastid, PfClpP
218 possesses a transit peptide that is cleaved by a putative stromal peptide peptidase in the
219 apicoplast[12]. A second cleavage event is required for the removal of the pro-domain through an
220 unknown mechanism. It is possible that another protease is responsible for PfClpP pro-domain
221 cleavage or that this is an autocatalytic event. It is unknown how these processing events
222 influence complex assembly and maturation of the protease. To address all of these questions

223 and to understand the mechanism of PfClpP oligomerization, we specifically interfered with
224 the proteolytic activity of PfClpP *in vivo*.
225 For this purpose, we designed a PfClpP dead-protease mutant (termed PfClpP^{DEAD}) with a
226 point mutation in the protease active site (Ser264Ala) that renders it catalytically inactive[27]
227 (Figure 4A). It also includes the swapping of two residues (Glu308Arg/ Arg285Glu) of an ion pair
228 at the interface of the ClpP subunits[28]. The purpose of this switch is to reduce the affinity
229 between PfClpP^{DEAD} and the endogenous PfClpP in order to minimize a potential dominant
230 negative effect which may prevent us from studying PfClpP maturation and oligomerization.
231 We used the Hsp110 expression system to express this Ty-tagged PfClpP^{DEAD} mutant in
232 PfClpP^{apt} parasites (Figure 4A). The PfClpP^{DEAD} mutant co-localized in the apicoplast with
233 PfClpP^{apt} (Figure 4B). Western blot analysis showed that the PfClpP^{DEAD} is processed similarly
234 to the wild type PfClpP^{apt} to produce the cytoplasmic fraction (I); apicoplast-localized zymogen
235 (II) and active protease without the pro-domain (III) (Figure 4C). However, a close examination
236 revealed that the proteolytic maturation of the endogenous PfClpP^{apt} was reduced in the
237 presence of the PfClpP^{DEAD} variant. In the parental PfClpP^{apt} parasite line, the majority of the
238 apicoplast localized PfClpP zymogen was cleaved (fraction III, see 'parental' in Figure 4C). In
239 contrast, the processing of the same endogenous V5 tagged PfClpP was inhibited in the
240 PfClpP^{DEAD} parasites (Figure 4C). Quantification of the ratio between the processed (III) and the
241 zymogen (II) fractions, revealed a decrease of about 70% in the proteolytic processing of
242 PfClpP^{apt} (Figure 4D).
243 The shift in the processing rate could be explained by competitive binding between the two
244 PfClpP alleles. To test this model, we co-immunoprecipitated the endogenous PfClpP^{apt} (V5
245 tag) and the PfClpP^{DEAD} (Ty tag). These experiments revealed that the two PfClpP alleles bind
246 each other, indicating that they hetero-oligomerize into a mixed complex (Figure 4E). This was
247 unexpected due to the swapping of the two residues (Glu308Arg/ Arg285Glu) of the ion pair at
248 the interface of the ClpP subunits. This cross-binding revealed several molecular features of
249 PfClpP activation; the ability of each protease variant to co-immunoprecipitate not only the
250 mature form (III) but also the zymogen (II) suggests that complex assembly precedes the final
251 processing step of removing the pro-domain (Figure 4E and 4H).

252

253 **PfClpP protease activity is essential for complex function**

254 The implication of the interaction between the wild-type and dead protease mutant became
255 apparent during PfClpP^{apt} knockdown; reducing the levels of the endogenous active protease
256 did not affect PfClpP^{DEAD} expression levels but it drastically inhibited its processing (Figure 4F).
257 The inability of the parasites to remove the pro-domain from the dead protease in the absence
258 of an active PfClpP, suggests that *in vivo* the PfClpP zymogen matures through trans-
259 autoprocessing (Figure 4H). These data further suggest that the PfClpP zymogen (II) is inactive
260 and this trans-autoprocessing is essential for PfClpP activation. These data support the model
261 that PfClpP zymogen forms oligomers, which may be required for trans-autoprocessing and
262 that the mechanism of maturation and oligomerization for plastid Clp proteases significantly
263 differs from their bacterial counterparts. Whether these are general features of ClpP zymogens
264 expressed in other plastids such as plant chloroplasts remains to be explored. Future structural
265 studies with the ClpP dead zymogens may reveal additional features such as whether the
266 zymogen is required to ensure proper trans-autocatalytic activity.

267 Importantly, the robust activity of PfClpP enabled the PfClpP^{DEAD} parasites to grow normally
268 despite the presence of the mixed complexes. However, the presence of the PfClpP^{DEAD}
269 mutant rendered them more sensitive to perturbations in PfClpP levels, and under these
270 settings, knockdown of endogenous PfClpP^{apt} via removal of aTc resulted in parasite death
271 (Figure 4G). Thus, the expression of PfClpP^{DEAD} under normal PfClpP levels revealed the
272 mechanisms of PfClpP oligomerization and maturation (Figure 4H). Upon PfClpP knockdown,
273 the lethal effects of the dead-protease proved that it is the capacity to degrade substrates that
274 is required for organelle biogenesis and parasite survival (Figure 4H).

275

276 **The adaptor protein PfClpS is essential for plastid biogenesis and parasite survival**

277 Our data show that the proteolytic activity of the apicoplast Clp complex is central to its
278 essential role in regulating plastid biogenesis. Therefore, it is essential to understand the
279 mechanisms by which the apicoplast ClpP/R/C complex recognizes its substrates.

280 Bioinformatic analysis have identified a putative substrate adaptor protein termed PfClpS, but
281 its localization and physiological functions have not yet been determined[29].
282 Therefore, we tagged PfClpS with a V5 tag and the *tetR*-aptamer knockdown system to
283 generate PfClpS^{apt} parasites, and confirmed integration by PCR (Figure 5A). We observed co-
284 localization of PfClpS and the apicoplast marker ACP (Figure 5C). Removal of aTc from
285 PfClpS^{apt} parasites led to a significant protein knockdown (Figure 5B). As a consequence, aTc
286 removal inhibited parasite growth, demonstrating that PfClpS is essential for parasite asexual
287 replication (Figure 5D). Importantly, this growth inhibition was completely rescued by addition
288 of IPP, linking the essential function of PfClpS to the apicoplast (Figure 5D). Microscopy
289 revealed that apicoplast proteins such as ACP accumulated in vesicle-like structures, and
290 quantitative Real Time PCR confirmed that the apicoplast genome disappears upon PfClpS
291 knockdown (Figure 5C and E). Collectively, these data show that PfClpS activity is essential for
292 parasite viability and, similar to other Clp proteins, it is required for apicoplast biogenesis.
293
294 **PfClpS associates with the Clp complex and putative substrates**
295 To examine the functional interaction between PfClpS and the Clp complex, we used the
296 PfClpS^{apt} parasites to pull down potential interactors. The immunoprecipitation and proteomic
297 analyses were performed as described earlier for PfClpP and PfClpR. Out of 39 identified
298 potential PfClpS interactors, 20 hits passed the high-confidence threshold, including PfClpR
299 (Figure 5F and Supplementary Table 1). Due to the predicted function of PfClpS, this list may
300 be enriched with putative Clp substrates. The PfClpS phenotypic data suggest that the
301 substrates selected for degradation by PfClpS are essential for apicoplast biogenesis. Including
302 the 20 PfClpS binding proteins to the PfClpP and PfClpR interactors that were identified
303 earlier, resulted in a list of 35 potential Clp interactors (Supplementary table 1). Interestingly,
304 we found a high degree of overlap between hits, with roughly 50% of them shared between at
305 least 2 different IPs (PfClpP/R/S) (Figure 5G). Of a specific interest, was a small group of 5 high-
306 confidence hits that were common between all 3 IPs (Figure 5G, Supplementary table 1). These
307 predicted apicoplast proteins include a thioredoxin peroxidase, a putative RNA
308 methyltransferase and a putative acyl transferase (Figure 2H and Supplementary table 1).

309 Interestingly, these Clp interactors involved in very distinct metabolic pathways (protein
310 folding, RNA metabolism and lipid biosynthesis), thus emphasizing the role of the *Plasmodium*
311 Clp complex as a master regulator of apicoplast biology.
312
313 **A model for proteostasis regulation by the apicoplast Clp complex**
314 To conclude, we propose a model in which the apicoplast organelle maintains a stable
315 proteome via protein degradation. This central function is required, among other things, for
316 organelle biogenesis, and is executed and regulated by the proteolytic Clp complex (Figure
317 6A). As a consequence, interfering with the function of different subunits of the complex leads
318 to organelle loss and parasite death. In the core of the Clp complex is PfClpP, a conserved
319 potent serine protease (Figure 6B). PfClpP is transported to the apicoplast as a zymogen,
320 which hetero-oligomerizes into a complex, and then matures into the active protease through
321 trans-autocatalytic processing. PfClpR is a non-catalytic subunit that physically interacts with
322 other complex subunits and may play a regulatory role. PfClpC is the chaperone that unfolds
323 proteins and feed them into the proteolytic core. It interacts with the mature PfClpP but not
324 with the zymogen, suggesting that it binds at a later step during complex assembly.
325 Nevertheless, this interaction is crucial for complex activity and parasite survival. Finally, a
326 small adaptor molecule, PfClpS, binds specific substrates and delivers them to the complex.
327 Targeting protein synthesis in the apicoplast is clinically effective, as manifested by the clinical
328 use of antibiotics such as doxycycline as antimalarials. However, such drugs inhibit the
329 production of only a small fraction of apicoplast proteins, as the majority of them are
330 transcribed by the cell nucleus and translated by the eukaryotic ribosomes in the parasite
331 cytoplasm. Thus, a broader and potentially more efficient way to disrupt the apicoplast
332 proteome would be to target its prokaryotic Clp degradation system. Indeed, due to their
333 central function in prokaryotes, the bacterial ClpP homologs lie in the center of various drug
334 discovery programs that identified potent inhibitors[30-34]. Ongoing work testing the
335 effectiveness and specificity of these bacterial inhibitors against PfClpP may lead to the
336 identification of antimalarials[15]. Our data and model suggest that small molecules inhibiting
337 PfClpP activity will have a dual effect of reducing substrate cleavage as well as preventing the

338 further production of the mature and active PfClpP. Future work is required to identify such
339 potent inhibitors because our data show, similar to its bacterial orthologs, the *Plasmodium* Clp
340 complex is an excellent drug target.

341 ## Materials &Methods

342 ### Plasmids construction

343 Genomic DNA was isolated from *P. falciparum* using the QIAamp DNA blood kit (QIAGEN). All
344 constructs utilized in this study were confirmed by sequencing. PCR products were inserted
345 into the respective plasmids using Sequence and Ligation Independent Cloning (SLIC). Briefly,
346 insert and cut vector were mixed with a T4 DNA polymerase and incubated for 2.5 minutes at
347 room temperature, followed by 10 minutes incubation on ice and then transformed into
348 bacteria. All restriction enzymes used for this study were purchased from New England
349 Biolabs. All oligonucleotides used in this study are in Supplemental Table 2.

350 For the generation of PfClpP^{KO} donor plasmid, 500 bp from the 5'UTR of *pfclpp*
351 (PF3D7_0307400) were amplified using primers 1+2 and 500 bp from the 3'UTR of *pfclpp* were
352 amplified using primers 3+4. The human dihydrofolate reductase (hDHFR) drug selection
353 cassette was amplified from pL6 vector using primers 5+6. All three pcr products were inserted
354 into a TOPO cloning vector (ThermoFisher). Primer 7 was used in combination with primer 6 or
355 4 to test for accurate integration in the parasite following transfections. To increase efficiency
356 of CRISPR/Cas9 mediated-integration, two guide RNAs were used, targeting both ends of the
357 PfClpP gene. For expression of a C-term PfClpP guide RNA, oligos 8+9 were inserted into
358 pUF1-Cas9-guide, and for expression of the N-term PfClpP guide RNA, oligos 10+11 were
359 independently inserted into pUF1-Cas9-guide as previously described[15,35].

360 For the generation of the PfClpP^{apt} conditional mutant, 500 bps from the 3'UTR and from the
361 C-term of *pfclpp* gene were amplified pClpP-glmS vector[15] using primers 18+19 and 20+21,
362 respectively. The two products were conjugated together using PCR-sewing and inserted as
363 one piece into pMG74-tetR-Dozi vector[24]. For expression of a C-term ClpP guide RNA, oligos
364 8+9 were inserted into pUF1-Cas9-guide.

365 For the generation of the PfClpR^{apt} conditional mutant, 500 bps from the 3'UTR and from the
366 C-term of *pfclpr* gene (PF3D7_1436800) were amplified from pClpR-glmS vector[15] using
367 primers 33+34 and 35+21, respectively. The two products were conjugated together using PCR-
368 sewing and inserted as one piece into pMG74-tetR-Dozi vector[24]. Primer 36 was used in
369 combination with primer 34 or 38 to test for accurate integration in the parasite following

370 transfections. Evaluating aptamer repeats numbers was done using primers 37+38. For
371 expression of a C-term PfClpR guide RNA, oligos 39+40 were inserted into pUF1-Cas9-guide.
372 For the generation of the PfClpS^{apt} conditional mutant, 500 bps from the 3'UTR and from the
373 C-term of *pfclps* gene (PF3D7_1320100) were amplified from gDNA using primers 41+42 and
374 43+44, respectively. The two products were conjugated together using PCR-sewing and
375 inserted as one piece into pMG74-tetR-Dozi vector[24]. Primer 45 was used in combination with
376 primer 42 or 38 to test for accurate integration in the parasite following transfections. For
377 expression of a C-term PfClpS guide RNA, oligos 46+47 were inserted into pUF1-Cas9-guide.
378 Primers 24+25 and 25+26 were used to test for accurate integration in the parasite following
379 transfections.
380 For the generation of the Hsp110 expression system, we designed a repair plasmid that
381 contains homology sequences from the *pfhsp110c* gene (PF3D7_0708800). The repair
382 sequences include the last 429 bp from *pfhsp110c* gene, followed by a 2A skip peptide, a
383 modular tagging cassette, and the first 400 bps from *pfhsp110c* 3'UTR. The modular tagging
384 cassette comprised of a multiple cloning site with several optional tags including mCherry, V5,
385 HA and Ty tags, allowing different tagging strategies using the same vector. The entire
386 construct was created using gene synthesis (GeneScript) and was cloned into a puc57
387 backbone to create the puc57-Hsp110 vector. For expression of a PfHsp110c guide RNA, oligos
388 22+23 were inserted into pUF1-Cas9-guide.
389 For the generation of tp^{ACP}-GFP parasites, tp^{ACP}-GFP was amplified from pCEN-tp^{ACP}-GFP
390 using primers 27+28, and was inserted into puc57-Hsp110 vector (cut with MfeI and SpeI) using
391 SLIC. For the generation of PfClpC^{wt} parasites, PfClpC (PF3D7_1406600) was amplified from
392 gDNA using primers 29+32. To introduce the point mutation required for the generation of
393 PfClpC^{F1103W} parasites, PfClpC was amplified from gDNA in two pieces, using primers 29+30
394 and 31+32. The two pieces were PCR-sewed together and inserted into puc57-Hsp110 vector
395 (cut with MfeI and NheI) using SLIC.
396 For the generation of PfClpP^{DEAD} parasites, we introduced the following point mutations into
397 the Open Reading Frame of PfClpP: Ser264Ala, Glu308Arg and Arg285Glu. The gene was

398 synthesized (GeneScrpit) and was inserted into puc57-Hsp110 vector (cut with MfeI and NheI)
399 using SLIC.

400 **Cell culture and transfections**

401 Parasites were cultured in RPMI medium supplemented with Albumax I (Gibco) and
402 transfected as described earlier[15,36,37].

403 To generate PfClpP^{KO} parasites, a mix of three plasmids was transfected into 3D7 parasites in
404 the presence or absence of 200uM Isopentynyl Pyrophosphate (IPP, Isoprenoids LC). The
405 plasmid mix contained the PfClpP^{KO} donor plasmid and the two pUF1-Cas9-PfClpP-guide (N-
406 terminal and C-terminal guides). Drug pressure was applied 48 hours post transfection using
407 2.5 nM WR99210 (Sigma) to select for parasites expressing hDHFR.

408 To generate PfClpP^{apt}, PfClpR^{apt} and PfClpS^{apt} parasites, a mix of two plasmids was transfected
409 into 3D7 parasites in the presence of 0.5 μM anhydrotetracycline (aTc, Cayman Chemicals).
410 The plasmid mix contained 50 μg of pUF1-Cas9-guide (expressing the relevant guide:
411 PfClpP/R/S) and 50 μg of the pMG74 based donor plasmid (with the related homology regions).
412 Drug pressure was applied 48 hours post transfection using 2.5 μg/ml Blasticidin (BSD, Sigma).
413 For each transfection, at least 2 clones were isolated via limiting dilution and used in all
414 subsequent experiments.

415 To generate tp^{ACP}-GFP, PfClpP^{DEAD}, PfClpC^{wt} and PfClpC^{F1103W} parasites, a mix of two plasmids
416 was transfected into PfClpP^{apt} parasites. For each different transfection the primers mix
417 contained 2 plasmids; 50 μg of pUF1-Cas9-PfHsp110c-guide and 50 μg of the relevant marker-
418 less puc57-Hsp110 repair plasmid (puc57-Hsp110-tp^{ACP}-GFP/ puc57-Hsp110-PfClpP^{DEAD}/ puc57-
419 Hsp110-PfClpC^{wt}/ puc57-Hsp110-PfClpC^{F1103W}, respectively). For PfClpC^{F1103W}, transfections
420 were performed in the presence or absence of 200 μM IPP (Isoprenoids LC). Drug pressure was
421 applied 48 hours post transfection, using 1μM DSM1 (BEI Resources), selecting only for Cas9
422 expression. DSM1 was removed from the culturing media once parasites clones were isolated
423 using limiting dilution.

424 **Growth assays**

425 For PfClpP^{apt}, PfClpP^{DEAD}, PfClpR^{apt} and PfClpS^{apt}, asynchronous parasite cultures were washed
426 5 times and incubated without aTc. For PfClpP^{KO} and PfClpC^{F1103W}, parasite cultures were

427 washed once and incubated without IPP. Throughout the course of the experiment parasites
428 were sub-cultured to maintain the parasitemia between 1-5% and parasitemia was monitored
429 every 24 hours via flow cytometry. Relative parasitemia at each time point was back calculated
430 based on actual parasitemia multiplied by the relevant dilution factors. Parasitemia in the
431 presence of aTc or IPP at the end of each experiment was set as the highest relative
432 parasitemia and was used to normalize parasites growth. Data were analyzed using Prism
433 (GraphPad Software, Inc.)
434 For IPP rescue (PfClpS^{apt}, PfClpP^{KO} and PfClpC^{F1103W}) media was supplemented with 200 μM of
435 IPP (Isoprenoids LC) in PBS.
436

437 **Western blot**

438 Western blots were performed as described previously[38]. Briefly, parasites were collected and
439 host red blood cells were permeabilized selectively by treatment with ice-cold 0.04% saponin
440 in PBS for 10 min, followed by a wash in ice-cold PBS. Cells were lysed using RIPA buffer,
441 sonicated, and cleared by centrifugation at 4°C. The antibodies used in this study were mouse
442 anti-GFP, JL8 (Roche, 1:3000), mouse anti-Ty SAB4800032 (Sigma, 1:1000), rabbit anti-V5,
443 D3H8Q (Cell Signaling, 1:1000), mouse anti-V5, TCM5 (eBioscience™, 1:1000), mouse
444 monoclonal anti-PMV (from D. Goldberg, 1:400), rabbit polyclonal anti-EF1α (from D.
445 Goldberg, 1:2000) and rabbit polyclonal anti-PfClpP (from W. Houry, 1:4000). The secondary
446 antibodies that were used are IRDye 680CW goat anti-rabbit IgG and IRDye 800CW goat anti-
447 mouse IgG (LICOR Biosciences, 1:20,000). The Western blot images and quantifications were
448 processed and analyzed using the Odyssey infrared imaging system software (LICOR
449 Biosciences).

450 **Microscopy and image processing**

451 For IFA cells were fixed using a mix of 4% Paraformaldehyde and 0.015% glutaraldehyde and
452 permeabilized using 0.1% Triton-X100. Primary antibodies used are mouse anti Ty1
453 SAB4800032 (Sigma, 1:500), rabbit anti-V5, D3H8Q (Cell Signaling, 1:100), mouse anti-V5,
454 TCM5 (eBioscience™, 1:100), rabbit anti-Cpn60 (from B. Striepen, 1:1,000) and rabbit anti-ACP
455 (from G. Mcfadden, 1:5,000). Secondary antibodies used are Alexa Fluor 488 and Alexa Fluor

456 546 (Life Technologies, 1:100). Cells were mounted on ProLong Diamond with DAPI
457 (Invitrogen). For live cell imaging of tp^{ACP}-GFP parasites were incubated with 8 μM Hoechst
458 (ThermoFisher Scientific) in PBS. The imaging was performed using DeltaVision II microscope
459 system with an Olympus IX-71 inverted microscope using a 100X objective. All images were
460 collected as Z-stack, were deconvolved using the DVII acquisition software SoftWorx and
461 displayed as maximum intensity projection. Image processing, analysis and display were
462 preformed using SoftWorx and Adobe Photoshop. Adjustments to brightness and contrast
463 were made for display purposes.

464 **Flow cytometry**

465 Aliquots of parasite cultures (5μl) were stained with 8 μM Hoechst (ThermoFisher Scientific) in
466 PBS. The fluorescence profiles of infected erythrocytes were measured by flow cytometry on a
467 CytoFlex S (Beckman Coulter, Hialeah, Florida) and analyzed by FlowJo software (Treestar,
468 Inc., Ashland, Oregon). The parasitemia data were fit to standard growth curve using Prism
469 (GraphPad Software, Inc.).

470 **Quantitative Real Time PCR**

471 Asynchronous parasites ($PfClpP^{KO}$ and $PfClpC^{F1103W}$) or Synchronized ring stage parasites
472 ($PfClpS^{apt}$) samples were collected and genomic DNA was purified using QIAamp blood kits
473 (Qiagen). Primers that amplify segments from genes encoded by nuclear or organelles
474 genomes were designed using RealTime qPCR Assay Entry (IDT). The following primer
475 sequences were used: *cht1* (nuclear)- 12+13; *tufA* (apicoplast)- 14+15; *cytb3* (mitochondria)-
476 16+17. Reactions contained template DNA, 0.5 μM of gene specific primers, and IQ™ SYBR
477 Green Supermix (BIORAD). Quantitative real-time PCR was carried out in triplicates and was
478 performed at a 2-step reaction with 95°C denaturation and 56°C annealing and extension for 35
479 cycles on a CFX96 Real-Time System (BIORAD). Relative quantification of target genes was
480 determined using Bio-Rad CFX manager 3.1 software. Standard curves for each primers set
481 were obtained by using different dilutions of control gDNA as template, and were used to
482 determine primers efficiency. The organelle: nuclear genome ratio of mutant parasites was

483 calculated relative to that of the control. Unpaired t-test (Benjamini, Krieger, Yekutieli) was
484 used to calculate significance between control and mutants.
485
486 **Immunoprecipitation**
487 For the pull-down proteomic analysis of PfClpP^{apt}, PfClpR^{apt} and PfClpS^{apt} parasites, the
488 parental line (wild type clone 3D7) was used a control and all pulldown experiments were done
489 in duplicates using two different clones. Immunoprecipitation protocols were performed using
490 anti-V5 antibody as previously described[39]. Briefly, pellets from 10^9 parasites were isolated
491 using cold saponin and were lysed and sonicated in Extraction Buffer (40 mM Tris HCL pH 7.6,
492 150 mM KCL, and 1 mM EDTA) supplemented with 0.5% NP-40 (VWR) and HALT protease
493 inhibitor (Thermo). 10% of the sample was kept for later analysis (input sample). Rabbit anti-V5
494 (Cell Signaling, D3H8Q) antibody was crosslinked to DynabeadsTM protein G (Invitrogen)
495 beads using 5 mM BS3 crosslinker (CovaChem) and then incubated with the supernatant at
496 4°C. Washes were performed using a magnetic rack (Life Technologies). Samples were run on
497 SDS-page and gel slices were sent to mass spectrometry analyses.
498 For the co-Immunoprecipitation of PfClpP^{DEAD} and PfClpP^{apt}, 2 samples of PfClpP^{DEAD} clone C9,
499 each containing 10^8 parasites were isolated as described above. Pellets were incubated with
500 either anti-Ty antibody (SAB4800032, Sigma) or with anti-V5 antibody (Cell Signaling,
501 D3H8Q). Input and IP samples were loaded on SDS-page and blotted with anti-Ty antibody
502 (SAB4800032, Sigma) or with anti-V5 (Cell Signaling, D3H8Q).
503 For the co-Immunoprecipitation of PfClpC^{wt} and PfClpP^{apt}, 2 samples of PfClpC^{wt}, each
504 containing 10^9 parasites were isolated as described above. Pellets were incubated with either
505 anti-Ty antibody (SAB4800032, Sigma) or with anti-V5 (Cell Signaling, D3H8Q) antibody. Input
506 and IP samples were loaded on SDS-page and blotted with Ty antibody (SAB4800032, Sigma)
507 or with anti-V5 (Cell Signaling, D3H8Q).
508
509 **Mass spectrometry and data analysis**
510 PfClpP^{apt}, PfClpR^{apt} and PfClpS^{apt} samples were sent to the proteomics shared resources in
511 Fred Hutchinson Cancer Research Center and were run on the OrbiDEAD Elite. The data were

512 searched using Proteome Discoverer 2.2 against the UP000001450 *Plasmodium falciparum*
513 (Uniprot Nov 2018) database including common contaminants using Sequest HT and
514 Percolator for validation. The search results were filtered for high confidence, with a strict 1%
515 false discovery rate.
516 All detected proteins were analyzed for predicted apicoplast localization using four different
517 bioinformatic algorithms: (i)PATS[40]; (ii)ApicoAP[41]; (iii)PlasmoAP[13]; and (iv) PlastNN[42]. We then
518 compared results from all four algorithms and used known apicoplast proteins (such as Clp
519 proteins) to estimate false-negative and false-positive rates for each algorithm. Based on these
520 data, we chose to filter for apicoplast prediction using PlasmoAP, since it had a lower false-
521 negative rate than PlastNN (higher sensitivity) and higher accuracy than the first two
522 algorithms. The abundance of each apicoplast-predicted protein was calculated by summing
523 the total intensities (MS1 values) of all matched peptides for each selected protein, and
524 normalizing by the total summed intensity of all matched peptides in the sample, as previously
525 described[42]. The resulted calculated value was then averaged between replicates. To filter for
526 high confidence hits, we calculated the abundance ratio between Clp IP (PfClpP/ PfClpR/
527 PfClpS) and the parental control, and set a threshold of $\geq$5 fold enrichment.

528 **ACKNOWLEDGMENTS**

529 We thank Geoffrey McFadden for anti-ACP antibody, Boris Striepen for anti-CPN60 antibody,
530 Walid Houry for anti-PfClpP antibody, and Dan Goldberg for anti-PMV, and anti-EF1α
531 antibodies; Julie Nelson at the CTEGD Cytometry Shared Resource Laboratory for help with
532 flow cytometry and analysis; and Muthugapatti Kandasamy at the Biomedical Microscopy Core
533 at the University of Georgia for help with microscopy. We acknowledge assistance of the
534 Proteomics Resource at Fred Hutchinson Cancer Research Center for mass spectrometry. This
535 work was supported the American Heart Association Postdoctoral Fellowship to A. F., and the
536 U.S. National Institutes of Health (R21AI128195) to V. M.

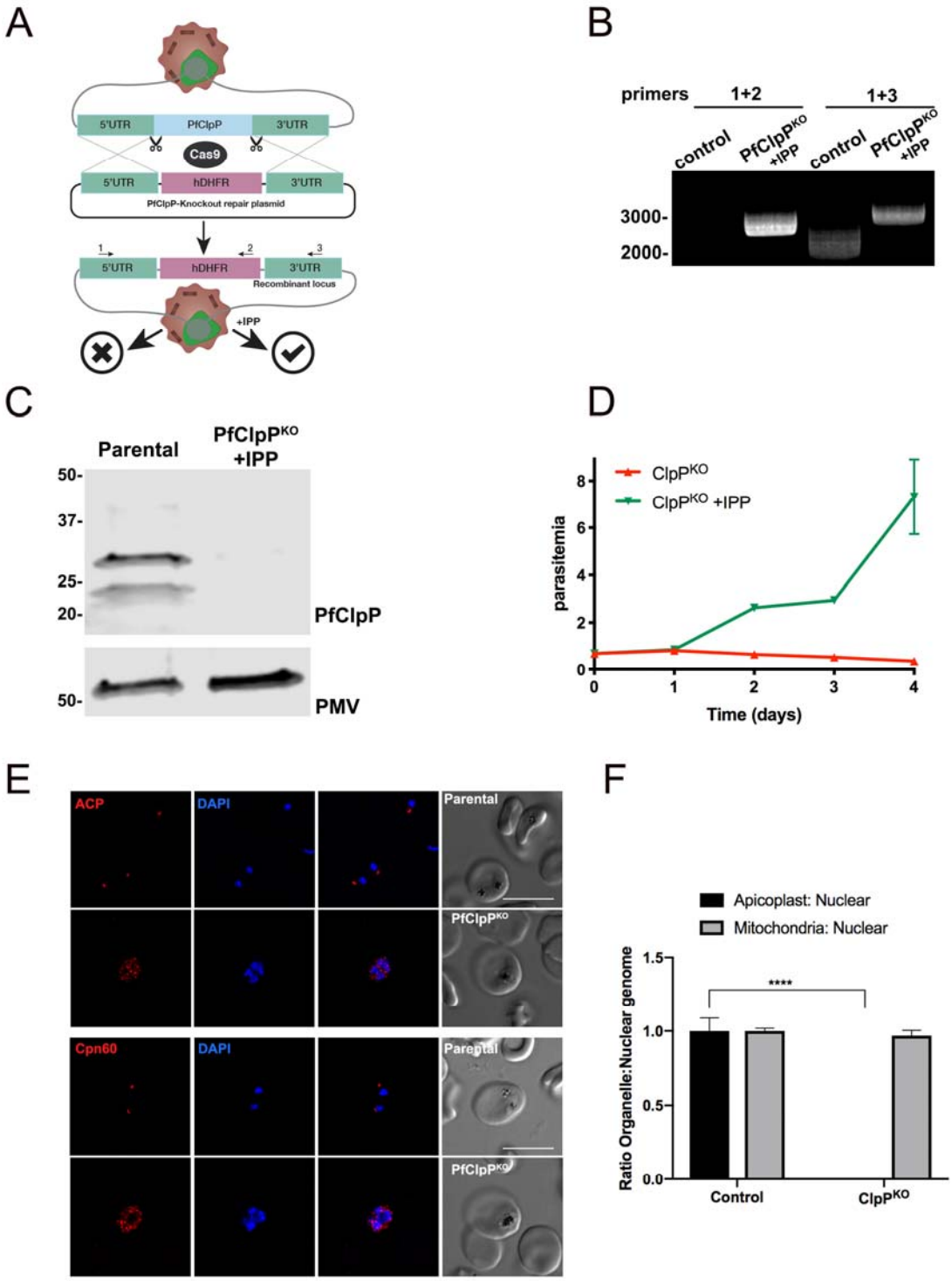
A
5'UTR
PfClpP
3'UTR
Cas9
5'UTR
hDHFR
3'UTR
PfClpP-Knockout repair plasmid
1
2
3
5'UTR
hDHFR
3'UTR
Recombinant locus
+IPP
B
primers
1+2
1+3
control
PfClpP^KO +IPP
control
PfClpP^KO +IPP
3000-
2000-
C
Parental
PfClpP^KO +IPP
50-
37-
25-
20-
PfClpP
50-
PMV
D
ClpP^KO
ClpP^KO +IPP
parasitemia
0
2
4
6
8
0
1
2
3
4
Time (days)
E
ACP
DAPI
Parental
PfClpP^KO
Cpn60
DAPI
Parental
PfClpP^KO
F
Apicoplast: Nuclear
Mitochondria: Nuclear
Ratio Organelle:Nuclear genome
1.5
1.0
0.5
0.0
****
Control
ClpP^KO

537

538 **Figure 1**

539 A. Generation of PfClpP knockout (PfClpP^{KO}) parasites. CRISPR/Cas9 and two guide RNAs
540 (gRNA) targeting the N- and the C-termini of PfClpP were used to facilitate integration.
541 The repair plasmid contained 500bps homology regions to the 5'UTR and the 3'UTR of the
542 *pfclpp* locus flanking the human dihydrofolate reductase selection marker (hDHFR).
543 Through double crossover integration and drug selection, the gene was replaced with the
544 drug marker. This strategy failed to retrieve live parasites unless IPP was added during drug
545 selection.

546 B. PCR test confirming hDHFR integration at the *pfclpp* locus in the presence of IPP. Genomic
547 DNA was purified from transfected parasites. Primers 1+2 (see methods) were used to
548 amplify an integration specific product. Primers 1+3 were used to amplify the region
549 between the 5'UTR and 3'UTR of *pfclpp*, as illustrated in A. A shift of 1 KB corresponds to
550 the integration of the hDHFR cassette.

551 C. Western blot of parasite lysates from parental line and PfClpP^{KO} parasites probed with
552 antibodies against PfClpP and Plasmepsin V (PMV, loading control), confirming loss of
553 PfClpP expression in the null mutants. The protein marker sizes that co-migrated with the
554 probed protein are shown on the left.

555 D. IPP was removed from PfClpP^{KO} parasites and parasitemia was monitored every 24 hours
556 over 4 days via flow cytometry. Data are represented as mean ± S.E.M. (n=3 technical
557 replicates). One representative experiment out of three biological replicates is shown.

558 E. Immunofluorescence imaging of fixed PfClpP^{KO} parasites stained with antibodies against
559 ACP (Acyl Carrier Protein), and DAPI (upper panel) or Cpn60 (Chaperonin 60) and DAPI
560 (lower panel). Both ACP and Cpn60 lose their typical apicoplast localization in PfClpP^{KO} and
561 appear in vesicle-like structures. Z-stack images were deconvolved and projected as a
562 combined single image. Representative images from biological replicates are shown. Scale
563 bar, 5µm.

564 F. Genomic DNA samples were collected from PfClpP^{KO} and control parasites for quantitative
565 Real Time PCR analysis. Apicoplast: nuclear genome ratio was calculated for each sample.
566 Mitochondria: nuclear genome ratio served as a control. Genome ratios were normalized to

567 control parasites. Apicoplast genome is completely lost in PfClpP^{KO} mutants, while the
568 mitochondria genome was unaffected. One representative experiment (out of 3 biological
569 replicates) is shown. Data are represented as mean ± S.E.M (n=3 technical replicates,
570 unpaired t-test, P value =0.00013)

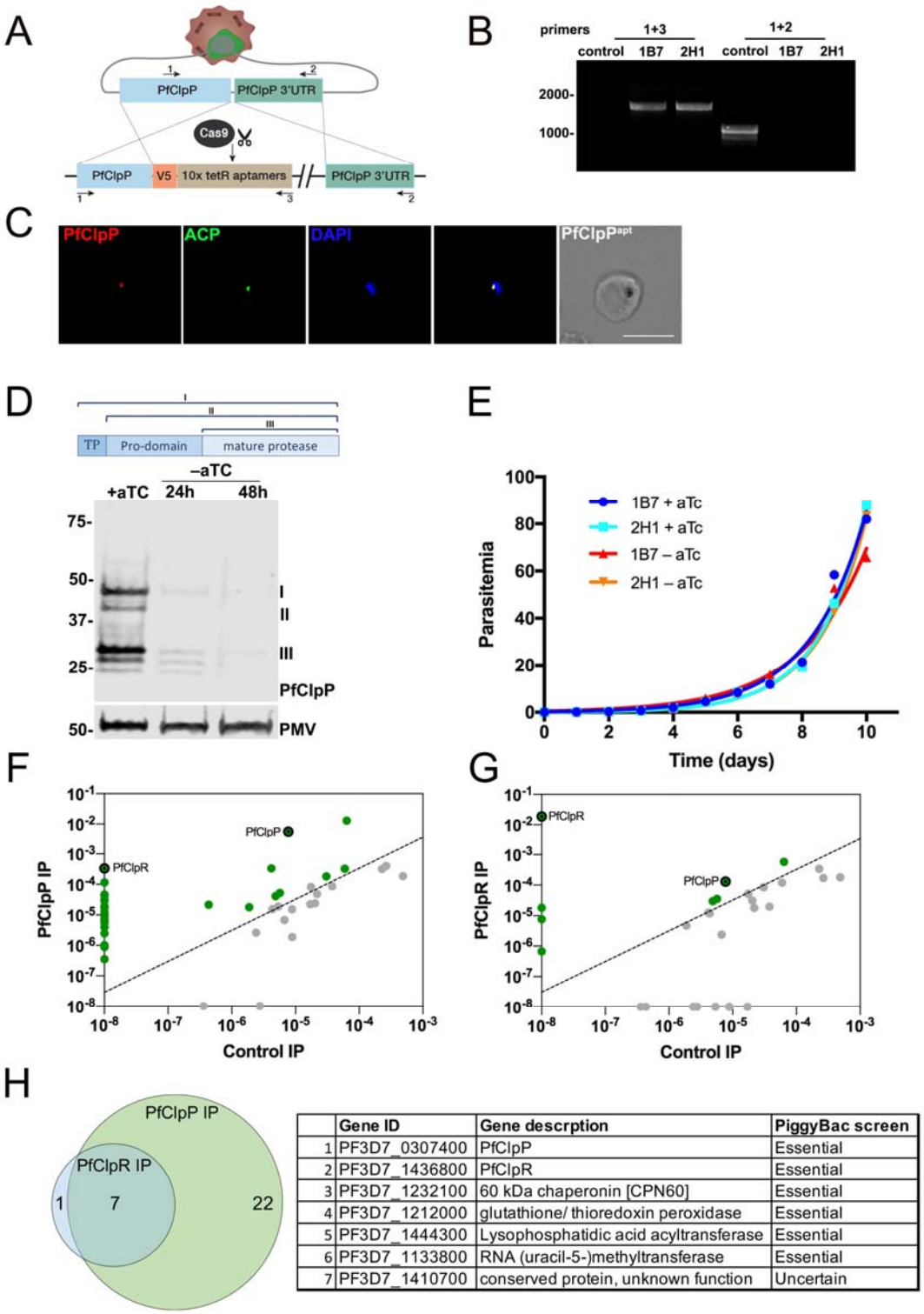

	Gene ID	Gene descrption	PiggyBac screen
1	PF3D7_0307400	PfClpP	Essential
2	PF3D7_1436800	PfClpR	Essential
3	PF3D7_1232100	60 kDa chaperonin [CPN60]	Essential
4	PF3D7_1212000	glutathione/ thioredoxin peroxidase	Essential
5	PF3D7_1444300	Lysophosphatidic acid acyltransferase	Essential
6	PF3D7_1133800	RNA (uracil-5-)methyltransferase	Essential
7	PF3D7_1410700	conserved protein, unknown function	Uncertain

571

572

573 **Figure 2**

574 A. Diagram showing integration of the *tetR*-aptamer system into the *pfclpp* locus. The Cas9
575 nuclease together with a PfClpP-specific gRNA introduces a double-stranded break at the
576 C-terminus of the *pfclpp* gene. The repair plasmid provides the template for double-
577 crossover homologous recombination, introducing a 3xV5 tag and the *tetR-Dozi* cassette,
578 including 10 aptamer repeats.

579 B. PCR test confirming *tetR-Dozi* integration at the *pfclpp* locus. gDNA was purified from 2
580 independently selected mutant clones (1B7 and 2H1). Primers 1,2,3 (see methods) were
581 used to amplify the native locus (1+2) or an integration specific product (1+3), as illustrated
582 in the diagram in A.

583 C. Immunofluorescence imaging of fixed PfClpP^{apt} parasites clone 1B7 stained with antibodies
584 recognizing PfClpP (anti-V5, red), ACP (anti-Acyl Carrier Protein, green), and DAPI. Z-stack
585 images were deconvolved and projected as a combined single image. Representative
586 images from three biological replicates are shown. Scale bar, 5μm.

587 D. PfClpP^{apt} parasites were incubated without aTc for 2 days, and lysates were isolated every
588 24 hr. Western blot shows parasite lysates probed with antibodies recognizing PfClpP (anti-
589 V5) and Plasmepsin V (anti-PMV, loading control). The expected processing pattern of
590 PfClpP is depicted: cytoplasmic fraction (I); apicoplast-localized zymogen (II) and mature
591 protease after removal of the pro-domain (III). A significant reduction in PfClpP protein
592 levels in achieved after 24 hours. The protein marker sizes that co-migrated with the
593 probed protein are shown on the left.

594 E. Two independent mutant clones (1B7 and 2H1) of PfClpP^{apt} parasites were grown with or
595 without 0.5 μM aTc, and parasitemia was monitored every 24 hr over 11 days via flow
596 cytometry. 100% of growth represents the highest value of calculated parasitemia (final
597 parasitemia in the presence of aTc). Data are fit to an exponential growth equation and are
598 represented as mean ± SEM (n= 3 technical replicates). One representative experiment out
599 of three biological replicates is shown.

600 F. Mass spectrometry analysis of PfClpP Immunoprecipitate, isolated from PfClpP^{apt} parasite
601 lysates using anti V5 antibody-conjugated beads. The parental line 3D7 was used a control

602 and pulldown experiments were done in duplicates using two independent PfClpP^{apt}
603 clones; 1B7 and 2H1. All proteins detected in both biological replicates were filtered for
604 predicted apicoplast localization. The abundance of each apicoplast-predicted protein was
605 calculated and averaged between replicates. To filter for high confidence hits, we set a
606 threshold of ≥5 fold enrichment in Clp IP vs. parental control. For PfClpP, 29 out of 45
607 proteins have passed the threshold and were defined as high-confidence hits, including
608 PfClpR.

609 *G*. PfClpR was immunoprecipitated from lysates of PfClpR^{apt} parasites using anti V5 antibody-
610 conjugated beads. Biological replicates were performed for both parental control and
611 PfClpR^{apt} parasites (Clones A10 and B5). The sample analysis and data were processed as in
612 F and 8 out of 29 hits passed the threshold, including PfClpP.

613 H. Venn diagram and a table showing the overlap between proteins identified in PfClpP and
614 PfClpR pulldowns. Out of the 8 PfClpR positive hits, 7 were also found in the PfClpP list,
615 outlining them as high confidence interactors.

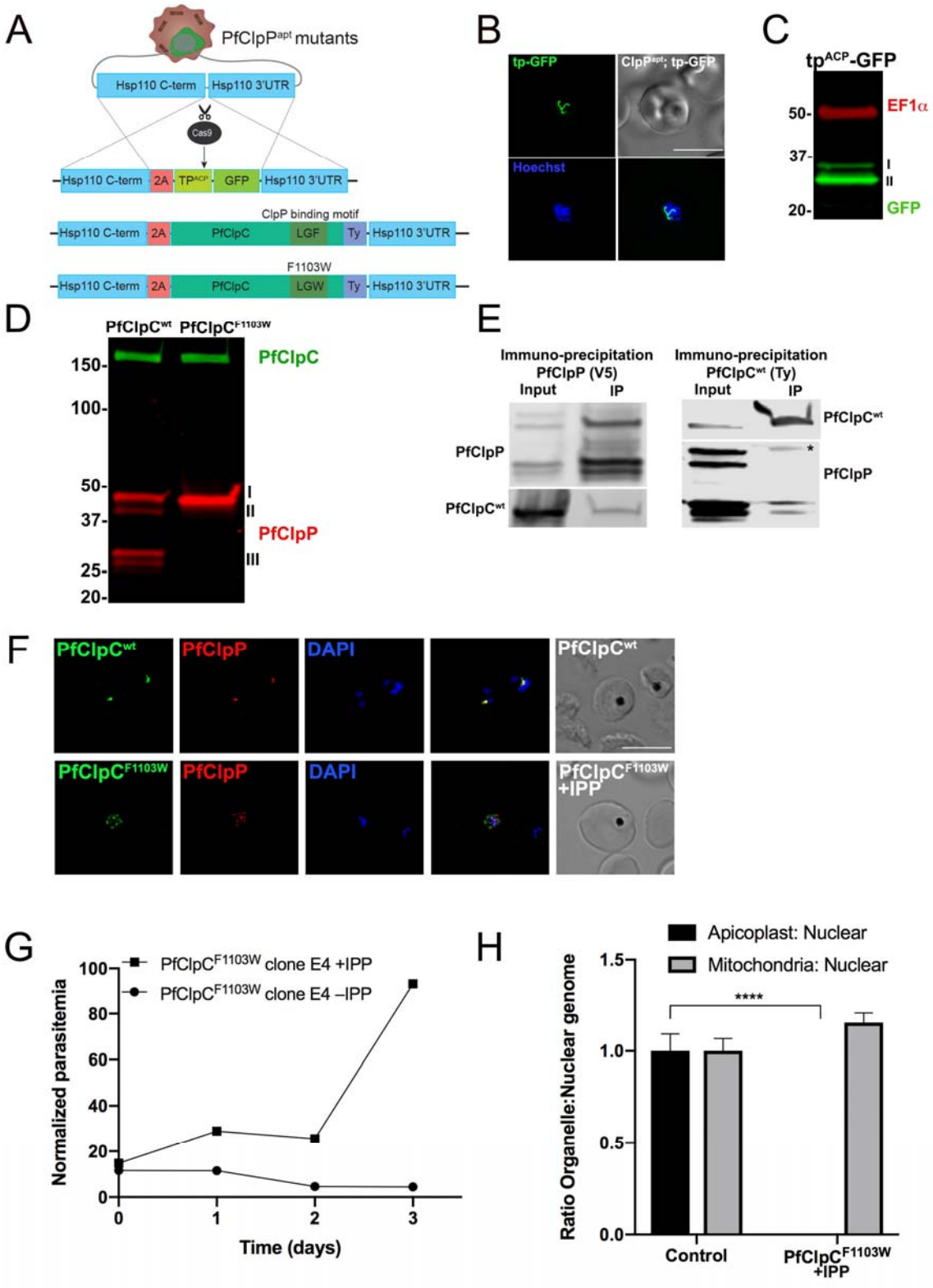
A
PfClpP^apt mutants
Hsp110 C-term
Hsp110 3'UTR
Cas9
2A
TP^ACP
GFP
ClpP binding motif
PfClpC
LGF
Ty
F1103W
LGW
B
tp-GFP
ClpP^apt; tp-GFP
Hoechst
C
tp^ACP-GFP
EF1α
GFP
D
PfClpC^wt
PfClpC^F1103W
PfClpC
PfClpP
E
Immuno-precipitation PfClpP (V5)
Immuno-precipitation PfClpC^wt (Ty)
Input
IP
PfClpP
PfClpC^wt
F
DAPI
PfClpC^F1103W +IPP
G
PfClpC^F1103W clone E4 +IPP
PfClpC^F1103W clone E4 –IPP
Normalized parasitemia
Time (days)
H
Apicoplast: Nuclear
Mitochondria: Nuclear
Ratio Organelle:Nuclear genome
Control
PfClpC^F1103W +IPP

616
617

618 **Figure 3**

619 A. Diagram showing integration and expression through the Hsp110 expression system. Cas9
620 nuclease together with a gRNA targeting the *pfhsp110c* locus, introduces a double-
621 stranded break at the c-terminus of the *pfHsp110c* gene. The repair plasmid provides two
622 homology regions for homologous recombination, flanking a 2A skip peptide and a tagged
623 gene of interest. Using this method, we introduced an apicoplast-localized GFP, a copy of
624 wild type PfClpC tagged with 3xTy (PfClpC^{wt}) and a PfClpC variant with a mutation in the
625 putative PfClpP binding site (PfClpC^{F1103W}).

626 B. Live fluorescence microscopy visualizing the apicoplast localized GFP (tp^{ACP}-GFP)
627 expressed through the *pfHsp110c* locus in PfClpP^{apt} parasites. Parasite DNA was stained
628 with Hoechst. Representative image from biological replicates is shown.

629 C. Western blot of parasite lysates from tp^{ACP}-GFP parasites probed with antibodies against
630 GFP and EF1α (loading control). The protein marker sizes that co-migrated with the probed
631 protein are shown on the left.

632 D. Western blot of parasite lysates from PfClpC^{wt} and PfClpC^{F1103W} parasites probed with
633 antibodies against V5 (PfClpP, red) and Ty (PfClpC, green). Loss of all processing of PfClpP
634 in PfClpC^{F1103W} parasites is due to apicoplast loss. The protein marker sizes that co-
635 migrated with the probed protein are shown on the left.

636 E. Co-Immunoprecipitation of PfClpP and PfClpC in PfClpP^{apt}; PfClpC^{wt} parasites. 10^9
637 parasites were isolated and pellets were incubated with either anti-V5 antibody-conjugated
638 beads (PfClpP pulldown, left) or anti-Ty antibody-conjugated beads (PfClpC pulldown,
639 rights). Input and IP samples were loaded on SDS-page and blotted with anti-Ty (PfClpC)
640 and anti-V5 (PfClpP) antibodies. An interaction between the protease and the chaperone is
641 observed. The residual heavy chain of the anti-Ty antibody that eluted with the IP sample
642 despite the cross linker is also denoted (*).

643 F. Immunofluorescence microscopy of fixed PfClpC^{wt} and PfClpC^{F1103W} parasites stained with
644 antibodies against V5 (PfClpP, red), Ty (PfClpC, green), and DAPI (DNA). The two proteins
645 co-localize in the apicoplast in PfClpC^{wt} parasites but appear in vesicle-like structures in
646 PfClpC^{F1103W} parasites. Z-stack images were deconvolved and projected as a combined

647 single image. Representative images from one of two biological replicates are shown.
648 Scale bar, 5μm.
649 G. IPP was removed from PfClpC^{F1103W} parasites and parasitemia was monitored every 24
650 hours over 3 days via flow cytometry. 100% of growth represents the highest value of
651 calculated parasitemia (final parasitemia in the presence of IPP). Data are represented as
652 mean ± S.E.M. (n=3). One representative experiment out of two biological replicates is
653 shown.
654 G. Genomic DNA samples were collected from PfClpC^{F1103W} and control parasites for
655 quantitative Real Time PCR analysis. Apicoplast: nuclear genome ratio was calculated for
656 each sample. Mitochondria: nuclear genome ratio served as a control. Genome ratios were
657 normalized to control parasites. Data are represented as mean ± S.E.M (n=3 technical
658 replicates, unpaired t-test, P value=0.00025). One representative experiment out of two
659 biological replicates are shown.

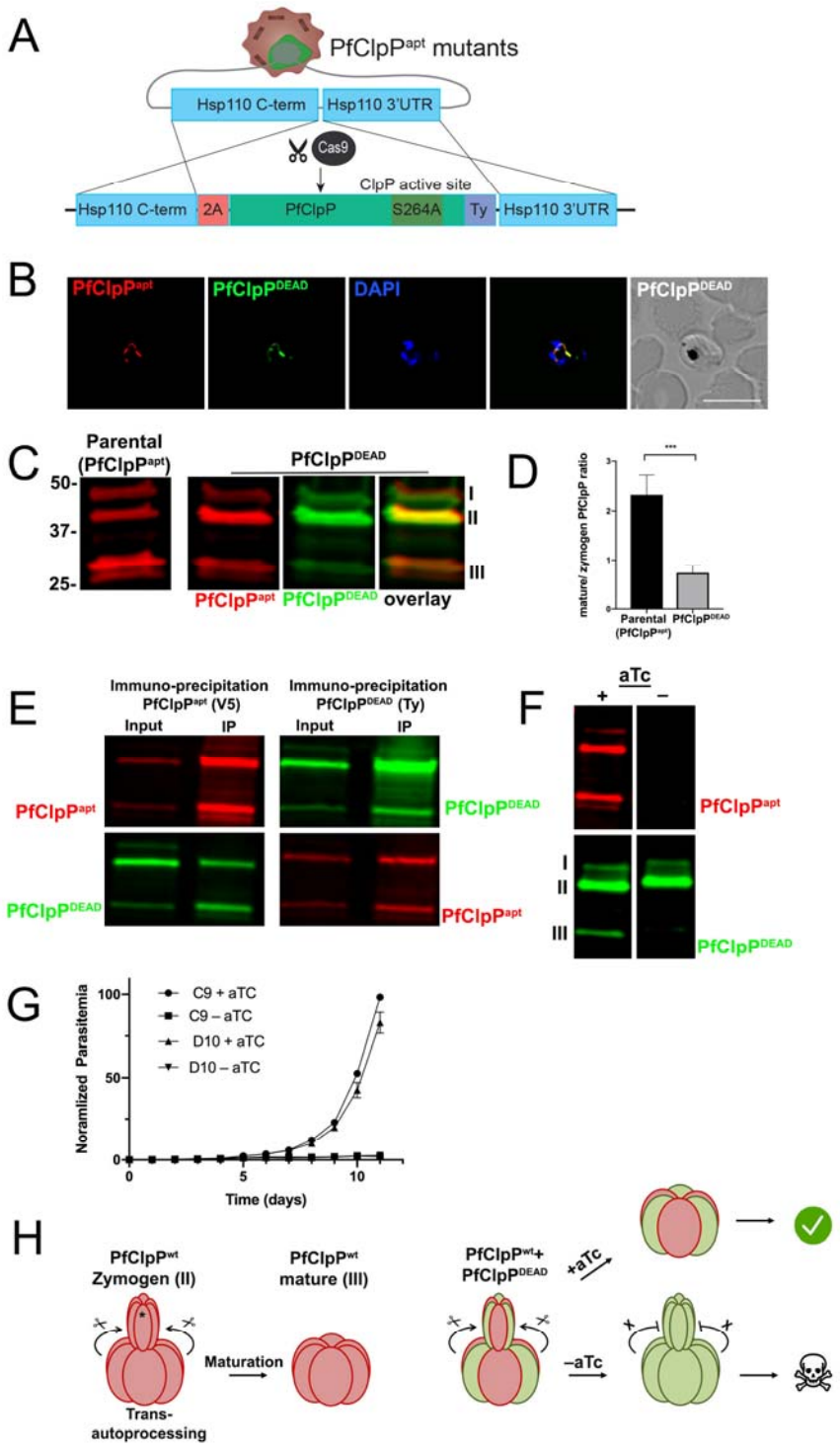
A
PfClpP^apt mutants
Hsp110 C-term
Hsp110 3'UTR
Cas9
ClpP active site
Hsp110 C-term
2A
PfClpP
S264A
Ty
Hsp110 3'UTR
B
PfClpP^apt
PfClpP^DEAD
DAPI
PfClpP^DEAD
C
Parental (PfClpP^apt)
PfClpP^DEAD
50-
37-
25-
I
II
III
PfClpP^apt
PfClpP^DEAD
overlay
D
mature/ zymogen PfClpP ratio
Parental (PfClpP^wt)
PfClpP^DEAD
E
Immuno-precipitation PfClpP^apt (V5)
Immuno-precipitation PfClpP^DEAD (Ty)
Input
IP
Input
IP
PfClpP^apt
PfClpP^DEAD
PfClpP^DEAD
PfClpP^apt
F
aTc
+
–
PfClpP^apt
I
II
III
PfClpP^DEAD
G
C9 + aTC
C9 – aTC
D10 + aTC
D10 – aTC
Noramlized Parasitemia
100
50
0
0
5
10
Time (days)
H
PfClpP^wt Zymogen (II)
PfClpP^wt mature (III)
Maturation
Trans-autoprocessing
PfClpP^wt+ PfClpP^DEAD
+aTc
–aTc

660

661 **Figure 4**

662 A. Diagram showing integration and expression of 3xTy-tagged PfClpP^{DEAD} variant into the
663 *pfHsp110c* locus. Cas9 nuclease in complex with a gRNA targeting this locus introduces a
664 double-stranded break at the C-terminus of the *pfHsp110c* gene. The repair plasmid
665 provides two homology regions for homologous recombination, flanking a 2A skip peptide
666 and the 3xTy-tagged PfClpP^{DEAD}. This catalytically-inactive PfClpP variant has a point
667 mutation in the protease active site (Ser264Ala).

668 B. Immunofluorescence microscopy of fixed PfClpP^{apt}; PfClpP^{DEAD} parasites stained with
669 antibodies against V5 (endogenous PfClpP^{apt}, red), Ty (PfClpP^{DEAD}, green) and DAPI (DNA).
670 The two proteins co-localize in the apicoplast. Z-stack images were deconvolved and
671 projected as a combined single image. Representative image from one of two biological
672 replicates is shown. Scale bar, 5µm.

673 C. Western blot of parental PfClpP^{apt} and PfClpP^{apt};PfClpP^{DEAD} parasite lysates probed with
674 antibodies against V5 (endogenous *wild type* PfClpP, red) and Ty (PfClpP^{DEAD}, green). The
675 identical migration pattern indicates that PfClpP^{apt} and PfClpP^{DEAD} are similarly processed.
676 The protein marker sizes that co-migrated with the probed protein are shown on the left.

677 D. The ratio between the mature and zymogen forms of endogenous PfClpP (V5-tagged) is
678 decreased upon PfClpP^{DEAD} expression, indicating that the dead variant interferes with the
679 processing of the endogenous protease. Quantification of the ratio of II and III fractions of
680 V5 tagged PfClpP from 3 biological replicates (p-value =0.0007, unpaired t-test).

681 E. Co-Immunoprecipitation of PfClpP^{apt} (V5-tagged) and PfClpP^{DEAD} (Ty-tagged). 10^8
682 parasites were isolated and pellets were incubated with either anti-V5 antibody-conjugated
683 beads (left) or anti-Ty antibody-conjugated beads (right). Input and IP samples were loaded
684 on SDS-page and blotted with anti-Ty and anti-V5 antibodies. The robust interaction
685 between the two Clp protease variants suggests that they hetero-oligomerize into a mixed
686 complex.

687 F. PfClpP^{apt};PfClpP^{DEAD} parasites were incubated without aTc for 24 hours, and lysates were
688 isolated. Western blot of these lysates was probed with antibodies against V5 (endogenous
689 PfClpP, red) and Ty (PfClpP^{DEAD}, green). PfClpP^{apt} knockdown results in the disappearance

690 of the processed form of PfClpP^{DEAD}, suggesting that the protease maturates through
691 trans-autoprocessing.

692 G. PfClpP^{apt};PfClpP^{DEAD} parasite clones (C9 and D10) were grown with or without aTc, and
693 parasitemia was monitored every 24 hr over 11 days via flow cytometry. 100% of growth
694 represents the highest value of calculated parasitemia (final parasitemia in the presence of
695 aTc). Data are represented as mean ± SEM (n=3 technical replicates). One representative
696 experiment out of two biological replicates is shown.

697 H. A model illustrating the mechanisms of PfClpP oligomerization and maturation. PfClpP
698 oligomerizes as a zymogen and subsequently matures by removing its pro-domain
699 (denoted with *) via trans-autoprocessing. In the presence of the PfClpP^{DEAD} variant, a
700 mixed complex is assembled and due to the robustness of PfClpP proteolytic activity, there
701 is no effect on parasite growth. Upon aTc removal expression levels of endogenous PfClpP
702 are dramatically reduced, and predominantly PfClpP^{DEAD} zymogen complexes are formed.
703 Consequently, substrate degradation is inhibited and the parasites die.

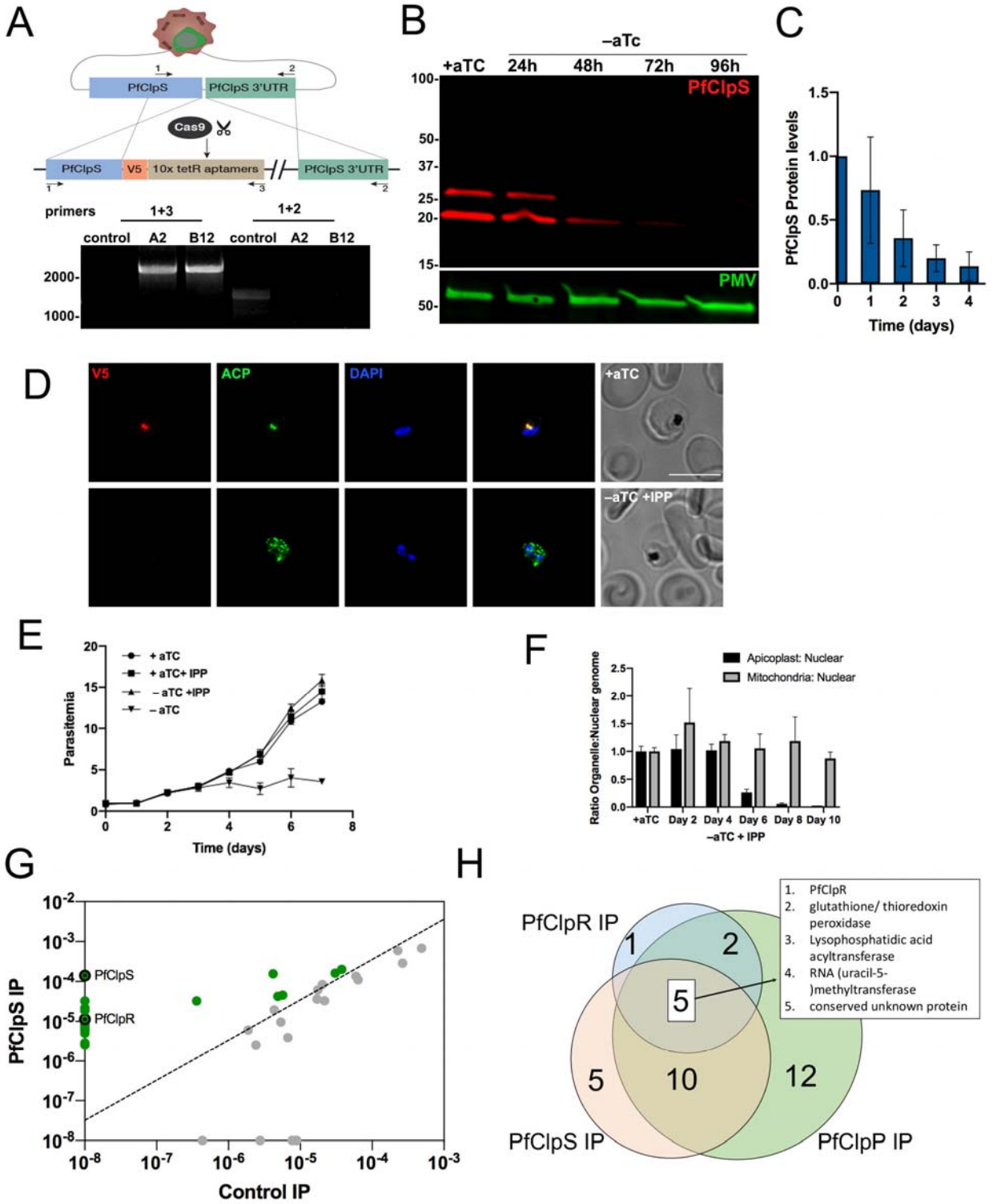
A
PfClpS
PfClpS 3'UTR
Cas9
PfClpS
V5
10x tetR aptamers
PfClpS 3'UTR
primers
1+3
1+2
control
A2
B12
control
A2
B12
2000-
1000-
B
–aTc
+aTC
24h
48h
72h
96h
PfClpS
PMV
100-
50-
37-
25-
20-
15-
50-
C
PfClpS Protein levels
Time (days)
D
V5
ACP
DAPI
+aTC
–aTC +IPP
E
+ aTC
+ aTC+ IPP
– aTC +IPP
– aTC
Parasitemia
Time (days)
F
Apicoplast: Nuclear
Mitochondria: Nuclear
Ratio Organelle:Nuclear genome
+aTC
Day 2
Day 4
Day 6
Day 8
Day 10
–aTC + IPP
G
PfClpS
PfClpR
PfClpS IP
Control IP
H
PfClpR IP
PfClpS IP
PfClpP IP
1
2
5
5
10
12
1. PfClpR
2. glutathione/ thioredoxin peroxidase
3. Lysophosphatidic acid acyltransferase
4. RNA (uracil-5-)methyltransferase
5. conserved unknown protein

704

705 **Figure 5**

706 A. Upper panel: Diagram showing integration of the *tetR*-aptamer cassette into the *pfclps*
707 locus. Cas9 nuclease with the gRNA introduces a double-stranded break at the beginning
708 of the C-terminus of the *pfclps* gene. The repair plasmid provides homology regions for
709 double-crossover homologous recombination, introducing a 3xV5 tag and the *tetR*-
710 aptamer cassette. Lower panel: PCR test confirming *tetR*-aptamer integration at the *pfclps*
711 locus. gDNA was purified from transfected parasites. Primers 1+2 or 1+3 (see methods)
712 were used to amplify the native locus or an integration specific band, as illustrated in the
713 diagram.

714 B. PfClpS^{apt} parasites were incubated without aTc for 4 days, and lysates were isolated every
715 24 hr. Western blot of parasite lysates probed with antibodies against V5 (PfClpS, red) and
716 Plasmepsin V (PMV, loading control, green). A significant reduction in PfClpS protein levels
717 in apparent after 72 hours. The protein marker sizes that co-migrated with the probed
718 protein are shown on the left.

719 C. Quantification of PfClpS knockdown (as shown in B, n= 3 biological replicates). Values were
720 normalized to PfClpS levels in the presence of aTc.

721 D. Immunofluorescence microscopy of fixed PfClpS^{apt} parasites that were incubated for 8 days
722 with aTc (upper panel) or without aTc and supplemented with IPP (lower panel). Parasites
723 were stained with antibodies against V5 (PfClpS, red), ACP (Acyl Carrier Protein, green),
724 and DAPI (DNA). PfClpS localizes to the apicoplast when aTc is present. Upon aTc removal,
725 PfClpS disappears and ACP appears in vesicle-like structures. Z-stack images were
726 deconvolved and projected as a combined single image. Representative images from one
727 of two biological replicates are shown. Scale bar, 5μm.

728 E. PfClpS^{apt} parasites (Clone A2) were grown with or without aTc and IPP, and parasitemia
729 was monitored every 24 hr over 7 days via flow cytometry. Parasites grown without aTc
730 exhibit a growth defect by day 4, and they die in the following days. Addition of IPP rescues
731 the growth defect, indicating an apicoplast damage. 100% of growth represents the
732 highest value of calculated parasitemia (final parasitemia in the presence of aTc). Data are

733 represented as mean ± SEM (n= 3 technical replicates). One representative experiment out
734 of three biological replicates is shown.

735 F. Synchronized PfClpS^{apt} parasites were grown in the absence of aTc and presence of IPP.
736 Genomic DNA samples were taken at the beginning of each replication cycle for real-time
737 qPCR analysis. Apicoplast: nuclear genome ratio was calculated every 48h. Mitochondria:
738 nuclear genome ratio served as a control. Genome ratios were normalized to parasites
739 grown in the presence of aTc. Data are represented as mean ± SEM (n= 3 technical
740 replicates). One representative experiment out of three biological replicates is shown.

741 G. Mass spectrometry analysis of PfClpS immunoprecipitated from PfClpS^{apt} parasites using
742 anti V5 antibody-conjugated beads. The parental line 3D7 was used a control and pulldown
743 experiments were done in duplicates. 10^9 parasites pellets were isolated and incubated
744 with anti-V5 crosslinked-beads. Samples were analyzed by mass spectrometry. All
745 detected proteins detected in biological replicates were filtered for predicted apicoplast
746 localization. The abundance of each apicoplast-predicted protein was calculated and
747 averaged between replicates. To filter for high confidence hits, we set a threshold of ≥5
748 fold enrichment in PfClpS vs. parental control. PfClpS IP yielded 30 apicoplast-localized
749 proteins, out of which 20 have passed the threshold and were defined as high-confidence
750 hits, including PfClpR.

751 H. Venn diagram showing the overlap between PfClpS, PfClpP and PfClpR high-confidence
752 interactors. Out of the 35-total high-confidence hits, 17 are shared between more than one
753 Clp IP and 5 proteins were identified in all 3 proteomic experiments

754

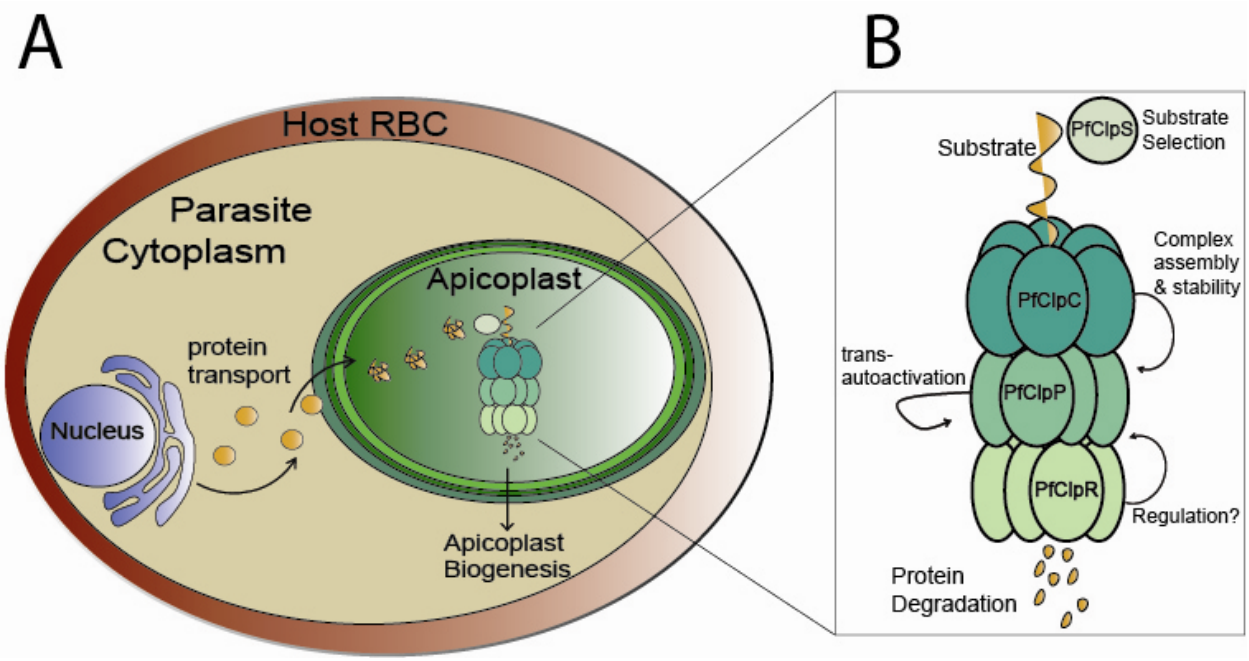

755 **Figure 6**

756 A. The Clp complex is a master regulator of apicoplast biology. Most of apicoplast proteins are
757 encoded by the cell nucleus, and are transported to the organelle via the secretory
758 pathway. According to this model, the apicoplast does not control their synthesis, and
759 therefore a stable proteome in the organelle is via protein degradation. This essential
760 function is required, among other things, for organelle biogenesis, and is executed and
761 regulated by the proteolytic Clp complex. As a consequence, interfering with the function
762 of different subunits of the complex leads to organelle loss and parasite death.

763 B. Molecular function of the apicoplast Clp system. In the core of the Clp complex is PfClpP, a
764 potent serine protease. PfClpP oligomerizes as a zymogen and then matures through
765 trans-autoprocessing. PfClpR is a non-catalytic subunit that interacts with other Clp
766 proteins and may have a regulatory role. PfClpC is the chaperone that unfolds proteins and
767 feed them into the PfClpP proteolytic core. A transient interaction between PfClpC and the
768 mature PfClpP is crucial for complex stability and function. A small adaptor molecule,
769 PfClpS, binds and selects specific substrates for delivery to the complex.

770

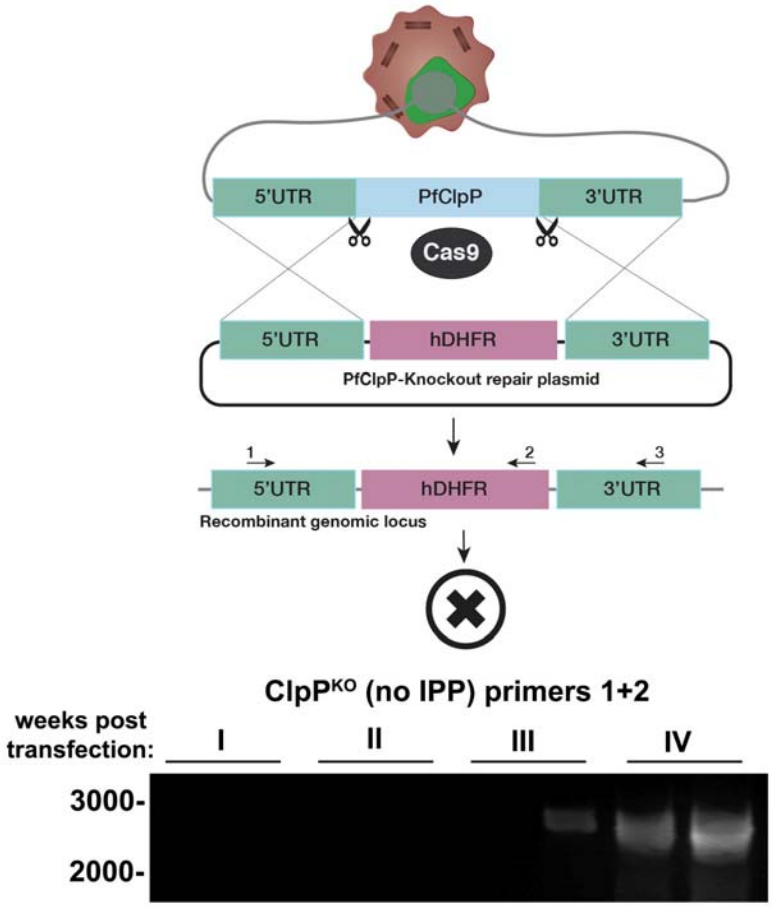

771
772
773 **Supplementary Figure 1**

774 A diagram depicting the generation of PfClpP knockout (PfClpP^{KO}) parasites. Cas9 nuclease
775 and two guide RNAs targeting the N- and the C-termini of PfClpP were used to facilitate
776 integration. The repair plasmid contained 500bps homology regions to the 5'UTR and the
777 3'UTR of the *pfclpp* locus flanking a drug marker (hDHFR, human Dihydrofolate Reductase).
778 Through double crossover integration and drug selection, the gene was replaced with the
779 drug marker. Despite evidence for integration into the genomic locus (bottom), this
780 strategy failed to retrieve live parasites in the absence of IPP, indicating the PfClpP is
781 essential to parasite viability due to its apicoplast function.

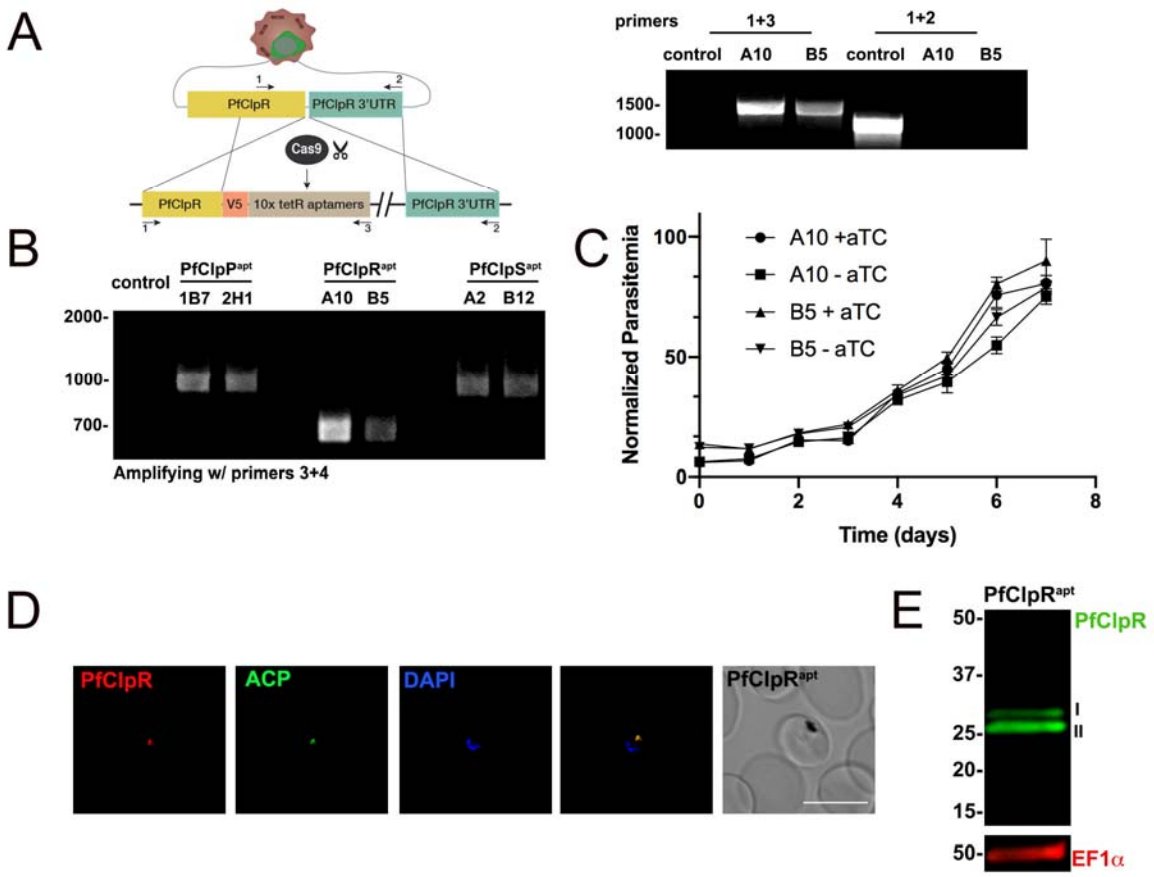

Supplementary Figure 2

A. Diagram showing integration of the *tetR*-aptamer system into the *pfclpr* locus. Cas9 nuclease with a specific guide RNA introduces a double-stranded break at the C-terminus of the *pfclpr* gene. The repair plasmid provides homology regions for double-crossover homologous recombination, introducing a 3xV5 tag and the *tetR*-aptamer cassette.

PCR test confirming *tetR-aptamer* integration at the *pfclpr* locus. Genomic DNA was purified from 2 mutant clones (A10 and B5). Primers 1,2,3 (see methods) were used to amplify the native locus (1+2) or an integration specific product (1+3), as illustrated in the diagram.

B. PCR test to evaluate aptamer repeat numbers in *tetR*-aptamer cassette in genomic DNA isolated from PfClpP^{apt}, PfClpR^{apt}, and PfClpS^{apt} clones. The original plasmid contained 10 aptamer repeats, each 100pb long. Reduction in repeats numbers implies decreased binding by the *tet*-Repressor which compromises knockdown efficiency. While PfClpP^{apt}

797 and PfClpS^{apt} clones show the expected 1 kb PCR product which corresponds to 10 aptamer
798 repeats, all PfClpR^{apt} clones show a 0.7 kb product, indicating the loss of 3 aptamer repeats.
799 C. Two PfClpR^{apt} clones (A5 and B10) were grown with or without 0.5 uM aTc, and parasitemia
800 was monitored every 24 hr over 11 days via flow cytometry. 100% of growth represents the
801 highest value of calculated parasitemia (final parasitemia in the presence of aTc). Data are
802 represented as mean ± SEM (n= 3 technical replicates). One representative experiment out
803 of two biological replicates is shown.
804 D. Immunofluorescence microscopy of fixed PfClpR^{apt} parasites stained with antibodies
805 against V5 (PfClpR^{apt}, red), ACP (Acyl Carrier Protein, green), and DAPI (DAPI). Z-stack
806 images were deconvolved and projected as a combined single image. Representative
807 images from one of two biological replicates are shown. Scale bar, 5µm.
808 E. PfClpR^{apt} lysates were isolated and probed with antibodies against V5 (PfClpR^{apt}, red), and
809 PMV (loading control). The doublet observed for PfClpR is typical for apicoplast proteins
810 and include a cytoplasmic fraction (I) and an apicoplast-localized protein after the transit
811 peptide had been removed (II). The protein marker sizes that co-migrated with the probed
812 protein are shown on the left.

813

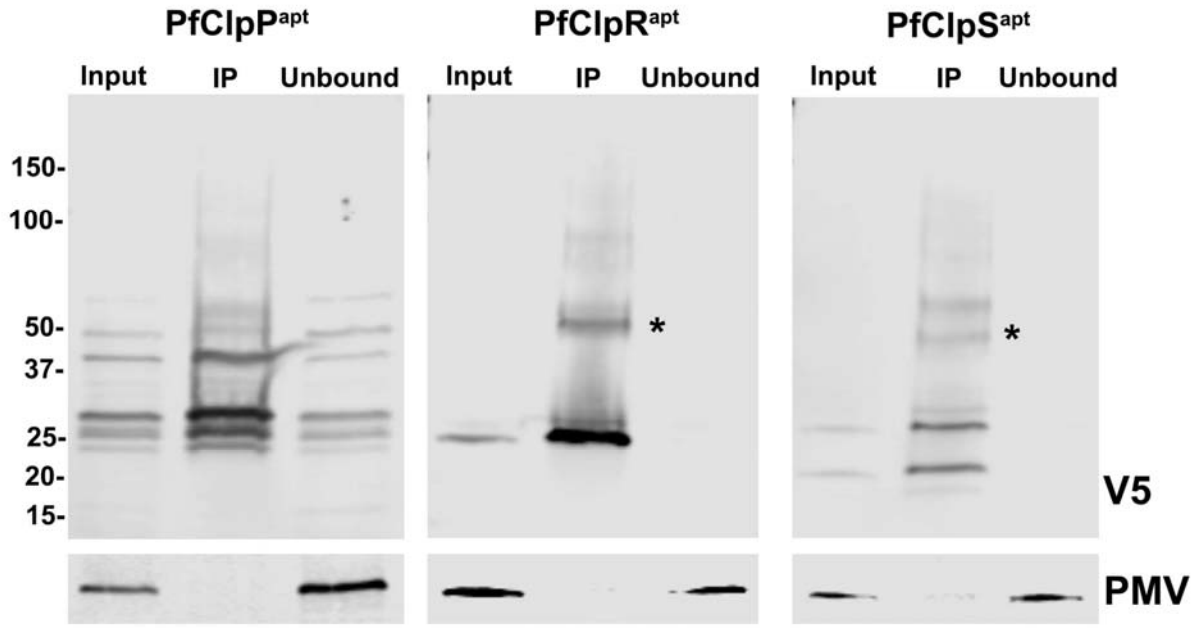

814 **Supplementary Figure 3**

815 Immunoprecipitation of PfClpP^{apt}, PfClpR^{apt} and PfClpS^{apt} for proteomic analysis. 10^9 parasites
816 were isolated and 10% of the volume was saved as an input sample. Immunoprecipitation of
817 the tagged proteins from respective parasite lysates were performed using anti-V5 antibody-
818 conjugated beads. Input, IP and unbound samples were separated on SDS-PAGE and blotted
819 with anti-V5 antibodies and anti-PMV (Plasmpesin V, loading control). The heavy chain of the
820 antibody that eluted with some of the IP samples, despite cross linking is shown (*).

821

822 ## References

823 1. McFadden, G. I. Plastid in human parasites. *Nature* **381,** 482–482 (1996).

824 2. Köhler, S., Delwiche, C. F., Denny, P. W., Tilney, L. G., Webster, P., Wilson, R. J., Palmer,
825 J. D. & Roos, D. S. A plastid of probable green algal origin in Apicomplexan parasites.
826 *Science* **275,** 1485–1489 (1997).

827 3. van Dooren, G. G. & Striepen, B. The algal past and parasite present of the apicoplast.
828 *Annu. Rev. Microbiol.* **67,** 271–289 (2013).

829 4. Ralph, S. A., Foth, B. J., Hall, N. & McFadden, G. I. Evolutionary Pressures on Apicoplast
830 Transit Peptides. *Mol Biol Evol* **21,** 2183–2194 (2004).

831 5. Fichera, M. E. & Roos, D. S. A plastid organelle as a drug target in apicomplexan
832 parasites. *Nature* **390,** 407–409 (1997).

833 6. Erica L Dahl, P. J. R. Multiple Antibiotics Exert Delayed Effects against the Plasmodium
834 falciparum Apicoplast. *Antimicrobial Agents and Chemotherapy* **51,** 3485–3490 (2007).

835 7. Borrmann, S., Issifou, S., Esser, G., Adegnika, A. A., Ramharter, M., Matsiegui, P.-B.,
836 Oyakhirome, S., Mawili-Mboumba, D. P., Missinou, M. A., Kun, J. F. J., Jomaa, H. &
837 Kremsner, P. G. Fosmidomycin-clindamycin for the treatment of Plasmodium
838 falciparum malaria. *J Infect Dis.* **190,** 1534–1540 (2004).

839 8. Sponer, U., Prajakwong, S., Wiedermann, G., Kollaritsch, H., Wernsdorfer, G. &
840 Wernsdorfer, W. H. Pharmacodynamic interaction of doxycycline and artemisinin in
841 Plasmodium falciparum. *Antimicrobial Agents and Chemotherapy* **46,** 262–264 (2002).

842 9. Dahl, E. L., Shock, J. L., Shenai, B. R., Gut, J., DeRisi, J. L. & Rosenthal, P. J. Tetracyclines
843 specifically target the apicoplast of the malaria parasite Plasmodium falciparum.
844 *Antimicrobial Agents and Chemotherapy* **50,** 3124–3131 (2006).

845 10. Goodman, C. D., Su, V. & McFadden, G. I. The effects of anti-bacterials on the malaria
846 parasite Plasmodium falciparum. *Molecular and Biochemical Parasitology* **152,** 181–191
847 (2007).

848 11. Waller, R. F., Reed, M. B., Cowman, A. F. & McFadden, G. I. Protein trafficking to the
849 plastid of Plasmodium falciparum is via the secretory pathway. *EMBO J* **19,** 1794–1802
850 (2000).

851 12. van Dooren, G. G., Su, V., D'Ombrain, M. C. & McFadden, G. I. Processing of an
852 Apicoplast Leader Sequence inPlasmodium falciparum and the Identification of a
853 Putative Leader Cleavage Enzyme. *Journal of Biological Chemistry* **277,** 23612–23619
854 (2002).
855 13. Foth, B. J., Ralph, S. A., Tonkin, C. J., Struck, N. S., Fraunholz, M., Roos, D. S., Cowman,
856 A. F. & McFadden, G. I. Dissecting Apicoplast Targeting in the Malaria Parasite
857 Plasmodium falciparum. *Science* **299,** 705–708 (2003).
858 14. Yeh, E. & DeRisi, J. L. Chemical rescue of malaria parasites lacking an apicoplast defines
859 organelle function in blood-stage Plasmodium falciparum. *PLoS Biol* **9,** e1001138 (2011).
860 15. Florentin, A., Cobb, D. W., Fishburn, J. D., Cipriano, M. J., Kim, P. S., Fierro, M. A.,
861 Striepen, B. & Muralidharan, V. PfClpC Is an Essential Clp Chaperone Required for
862 Plastid Integrity and Clp Protease Stability in Plasmodium falciparum. *Cell Rep* **21,** 1746–
863 1756 (2017).
864 16. Olivares, A. O., Baker, T. A. & Sauer, R. T. Mechanistic insights into bacterial AAA+
865 proteases and protein-remodelling machines. *Nat Rev Micro* **14,** 33–44 (2016).
866 17. Nishimura, K. & van Wijk, K. J. Organization, function and substrates of the essential Clp
867 protease system in plastids. *Biochimica et Biophysica Acta (BBA) - Bioenergetics* **1847,**
868 915–930 (2015).
869 18. Weber-Ban, E. U., Reid, B. G., Miranker, A. D. & Horwich, A. L. Global unfolding of a
870 substrate protein by the Hsp100 chaperone ClpA. *Nature* **401,** 90–93 (1999).
871 19. Kim, Y.-I., Levchenko, I., Fraczkowska, K., Woodruff, R. V., Sauer, R. T. & Baker, T. A.
872 Molecular determinants of complex formation between Clp/Hsp100 ATPases and the
873 ClpP peptidase. *Nature Structural & Molecular Biology* **8,** 230–233 (2001).
874 20. Frees, D., Gerth, U. & Ingmer, H. Clp chaperones and proteases are central in stress
875 survival, virulence and antibiotic resistance of Staphylococcus aureus. *International*
876 *Journal of Medical Microbiology* **304,** 142–149 (2014).
877 21. Rodríguez-Concepción, M., D'Andrea, L. & Pulido, P. Control of plastidial metabolism by
878 the Clp protease complex. *J. Exp. Bot.* **70,** 2049–2058 (2018).

879 22. Bakkouri, El, M., Pow, A., Mulichak, A., Cheung, K. L. Y., Artz, J. D., Amani, M., Fell, S.,
880 de Koning-Ward, T. F., Goodman, C. D., McFadden, G. I., Ortega, J., Hui, R. & Houry, W.
881 A. The Clp chaperones and proteases of the human malaria parasite Plasmodium
882 falciparum. *Journal of Molecular Biology* **404,** 456–477 (2010).
883 23. Bakkouri, El, M., Rathore, S., Calmettes, C., Wernimont, A. K., Liu, K., Sinha, D., Asad,
884 M., Jung, P., Hui, R., Mohmmed, A. & Houry, W. A. Structural insights into the inactive
885 subunit of the apicoplast-localized caseinolytic protease complex of Plasmodium
886 falciparum. *Journal of Biological Chemistry* **288,** 1022–1031 (2013).
887 24. Ganesan, S. M., Falla, A., Goldfless, S. J., Nasamu, A. S. & Niles, J. C. Synthetic RNA-
888 protein modules integrated with native translation mechanisms to control gene
889 expression in malaria parasites. *Nature Communications* **7,** 10727 (2016).
890 25. Wilson, R. H. & Hayer-Hartl, M. Complex Chaperone Dependence of Rubisco Biogenesis.
891 *Biochemistry* **57,** 3210–3216 (2018).
892 26. Muralidharan, V., Oksman, A., Pal, P., Lindquist, S. & Goldberg, D. E. Plasmodium
893 falciparum heat shock protein 110 stabilizes the asparagine repeat-rich parasite
894 proteome during malarial fevers. *Nature Communications* **3,** 1310 (2012).
895 27. Flynn, J. M., Neher, S. B., Kim, Y.-I., Sauer, R. T. & Baker, T. A. Proteomic discovery of
896 cellular substrates of the ClpXP protease reveals five classes of ClpX-recognition signals.
897 *Mol. Cell* **11,** 671–683 (2003).
898 28. Trentini, D. B., Suskiewicz, M. J., Heuck, A., Kurzbauer, R., Deszcz, L., Mechtler, K. &
899 Clausen, T. Arginine phosphorylation marks proteins for degradation by a Clp protease.
900 *Nature* **539,** 48–53 (2016).
901 29. AhYoung, A. P., Koehl, A., Vizcarra, C. L., Cascio, D. & Egea, P. F. Structure of a putative
902 ClpS N-end rule adaptor protein from the malaria pathogen Plasmodium falciparum.
903 *Protein Science* **25,** 689–701 (2016).
904 30. Gersch, M., Famulla, K., Dahmen, M., Göbl, C., Malik, I., Richter, K., Korotkov, V. S.,
905 Sass, P., Rübsamen-Schaeff, H., Madl, T., Brötz-Oesterhelt, H. & Sieber, S. A. AAA+
906 chaperones and acyldepsipeptides activate the ClpP protease via conformational
907 control. *Nature Communications* **6,** 6320 (2015).

908 31. Hackl, M. W., Lakemeyer, M., Dahmen, M., Glaser, M., Pahl, A., Lorenz-Baath, K.,
909 Menzel, T., Sievers, S., Böttcher, T., Antes, I., Waldmann, H. & Sieber, S. A. Phenyl
910 Esters Are Potent Inhibitors of Caseinolytic Protease P and Reveal a Stereogenic Switch
911 for Deoligomerization. *J. Am. Chem. Soc.* **137,** 8475–8483 (2015).
912 32. Brötz-Oesterhelt, H. & Sass, P. Bacterial caseinolytic proteases as novel targets for
913 antibacterial treatment. *International Journal of Medical Microbiology* **304,** 23–30 (2014).
914 33. Böttcher, T. & Sieber, S. A. β-Lactones as Specific Inhibitors of ClpP Attenuate the
915 Production of Extracellular Virulence Factors of Staphylococcus aureus. *J. Am. Chem.*
916 *Soc.* **130,** 14400–14401 (2008).
917 34. Conlon, B. P., Nakayasu, E. S., Fleck, L. E., LaFleur, M. D., Isabella, V. M., Coleman, K.,
918 Leonard, S. N., Smith, R. D., Adkins, J. N. & Lewis, K. Activated ClpP kills persisters and
919 eradicates a chronic biofilm infection. *Nature* **503,** 365–370 (2013).
920 35. Ghorbal, M., Gorman, M., Macpherson, C. R., Martins, R. M., Scherf, A. & Lopez-Rubio,
921 J.-J. Genome editing in the human malaria parasite Plasmodium falciparum using the
922 CRISPR-Cas9 system. *Nature Biotechnology* **32,** 819–821 (2014).
923 36. Cobb, D. W., Florentin, A., Fierro, M. A., Krakowiak, M., Moore, J. M. & Muralidharan, V.
924 The Exported Chaperone PfHsp70x Is Dispensable for the Plasmodium falciparum
925 Intraerythrocytic Life Cycle. *mSphere* **2,** e00363–17 (2017).
926 37. Kudyba, H. M., Cobb, D. W., Florentin, A., Krakowiak, M. & Muralidharan, V.
927 CRISPR/Cas9 Gene Editing to Make Conditional Mutants of Human Malaria Parasite P.
928 falciparum. *J Vis Exp* (2018). doi:10.3791/57747
929 38. Muralidharan, V., Oksman, A., Iwamoto, M., Wandless, T. J. & Goldberg, D. E.
930 Asparagine repeat function in a Plasmodium falciparum protein assessed via a
931 regulatable fluorescent affinity tag. *Proceedings of the National Academy of Sciences*
932 **108,** 4411–4416 (2011).
933 39. Kudyba, H. M., Cobb, D. W., Fierro, M. A., Florentin, A., Ljolje, D., Singh, B., Lucchi, N.
934 W. & Muralidharan, V. The endoplasmic reticulum chaperone PfGRP170 is essential for
935 asexual development and is linked to stress response in malaria parasites. *Cellular*
936 *Microbiology* **23,** e13042 (2019).

937 40. Zuegge, J., Ralph, S., Schmuker, M., McFadden, G. I. & Schneider, G. Deciphering
938 apicoplast targeting signals--feature extraction from nuclear-encoded precursors of
939 Plasmodium falciparum apicoplast proteins. *Gene* **280,** 19–26 (2001).
940 41. Cilingir, G., Broschat, S. L. & Lau, A. O. T. ApicoAP: the first computational model for
941 identifying apicoplast-targeted proteins in multiple species of Apicomplexa. *PLoS ONE*
942 **7,** e36598 (2012).
943 42. Boucher, M. J., Ghosh, S., Zhang, L., Lal, A., Jang, S. W., Ju, A., Zhang, S., Wang, X.,
944 Ralph, S. A., Zou, J., Elias, J. E. & Yeh, E. Integrative proteomics and bioinformatic
945 prediction enable a high-confidence apicoplast proteome in malaria parasites. *PLoS Biol*
946 **16,** e2005895 (2018).
947